(Proposal to Jefferson Lab PAC 30)

Measurement of the Ratio $R = \sigma_L/\sigma_T$ in Semi-Inclusive Deep-Inelastic Scattering

July 6, 2006

P. Bosted, W. Brooks, A. Bruell, V. Dharmawardane, R. Ent (spokesperson), D. Gaskell, T. Horn, M.K. Jones
Jefferson Lab, Newport News, VA 23606

I. Albayrak, M.E. Christy, C.E. Keppel, S. Malace, O. Oyebola H. Pushpakumari, L. Tang, V. Tvaskis, L. Yuan
Hampton University, Hampton, VA 23668

A. Asaturyan, A. Mkrtchyan, H. Mkrtchyan (spokesperson) T. Navasardyan, V. Tadevosyan
Yerevan Physics Institute, Yerevan, Armenia

W. Chen, H. Gao, X. Qian, X.F. Zhu
Duke University, Durham, NC 27708

P. Markowitz
Florida International University, University Park, FL 33199

G. Niculescu, I. Niculescu
James Madison University, Harrisonburg, VA 22807

D. Dutta
Mississippi State University, Mississippi State, MS 39762

G.M. Huber
University of Regina, Regina, Saskatchewan, Canada, S4S 0A2

X.D. Jiang
Rutgers, The State University of New Jersey, Piscataway, NJ 08855

Abstract

We propose to perform measurements of the ratio $R = \sigma_L/\sigma_T$ of longitudinal to transverse cross sections in pion electroproduction. Our emphasis will be on measurements in the so-called semi-inclusive deep inelastic scattering region, with extensions into the exclusive region.

Whereas inclusive scattering can not distinguish between the quark flavor, there is great promise in flavor decompositions of regular parton distributions through semi-inclusive deep inelastic scattering and of generalized parton distributions through deep exclusive scattering. For the latter, the ratio $R = \sigma_L/\sigma_T$ asymptotically scales like Q^2, the four-momentum transfer squared, at fixed Bjorken x. For the former, the ratio R is assumed to be similar to that of deep inelastic scattering.

Surprisingly, the latter assumption has never been thoroughly checked. Obviously, with less and less energy available to produce mesons, as is the case close to the exclusive limit (where the elasticity $z \to 1$), this assumption must locally fail. In fact, the ratio R for semi-inclusive pion electroproduction may at low energies depend on z, Q^2, or p_T, the transverse pion momentum. To measure this behavior, for the first time, is the subject of this proposal, for which we request 40 days of beam time.

The proposed measurements are both of fundamental and of practical value: They will allow us to study the inclusive-exclusive connection in pion electroproduction, a process where duality has recently been shown to be valid, and are a *sine qua non* for the interpretation of flavor decomposition by semi-inclusive deep inelastic scattering at a 12-GeV JLab (and other low-energy facilities).

We will detect charged pions ($\pi^{\pm}$) in coincidence with scattered electrons from semi-inclusive $(e, e'\pi)$ reaction on LH2 and LD2 targets at energies 6.6, 8.8 and 11.0 GeV, and beam currents of 50 μA. The Hall C HMS spectrometer and the projected SHMS with its first-generation detector package will be used for electron and meson detection.

Contents

I. INTRODUCTION

The electromagnetic interaction has proved very successful in probing the structure of the nucleon in a quest to understand the strong interactions between quarks and the gluons that bind them. In general, electron scattering experiments can be classified into inclusive, exclusive and semi-inclusive categories. In an inclusive electron scattering experiment, only the scattered electron is detected. In exclusive electron scattering, both the scattered electron and the full final hadronic state of the nucleon are detected (or, in the latter case, reconstructed by kinematics). In semi-inclusive scattering, one of the final-state hadrons is measured in coincidence with the scattered electron.

Considerable information on nucleon structure has been extracted over the past few decades from separations of inclusive lepton-nucleon cross sections, at high four-momentum transfer squared Q^2 and high excitation energy ν (corresponding to large missing mass W), into longitudinal and transverse structure functions. For example, early measurements of the structure function F_2 were shown to exhibit a (logarithmic) scaling behavior at fixed Bjorken $x = Q^2/2M\nu$. and were subsequently shown to be related to the momentum distribution of the quarks inside the nucleon in terms of parton distribution functions, whose universal nature makes them useful in understanding a wide variety of particle interactions with nucleons. Similarly, the original experimental observation of the smallness of the ratio $R = \sigma_L/\sigma_T$, the ratio of the contributions to the measured cross section from longitudinally and transversely polarized virtual photon scattering, respectively, as measured in deep inelastic scattering (DIS) provided the first evidence of the fundamental spin-1/2 nature of the partons.

Since that time, separated structure functions F_2 and R have been measured in DIS over a wide range of Q^2 and x, at CERN, SLAC, and DESY. More recently, the first precision separated measurements of the proton structure functions R and F_2 were performed at JLab, mainly emphasizing the nucleon resonance region but also extending into the DIS region.

It has been long realized that more stringent tests of the quark-parton model arise from inclusive hadron production experiments. Here, we will concentrate on the simplest of these, pion electroproduction. In the semi-inclusive process, there is great similarity with the inclusive process described above, but now there exists an additional kinematical degree of freedom associated with the momentum of the pion detected. With the positive z-axis in the direction of the electromagnetic current, two further variables can be chosen to characterize the problem: p_T and z. As a result, there will be in general four structure functions for the $(e, e'\pi)$ coincidence process, the usual longitudinal and transverse structure functions and two additional interference structure functions.

In the asymptotic limit, in the model where the electro-produced pions are the fragmentation products of spin-1/2 partons, the ratio $R = \sigma_L/\sigma_T$ disappears like $1/Q^2$, like in the inclusive case. This idea is supported by the measurement of angular distributions of hadrons in the process $e^+e^- \rightarrow h + X$, with h a hadron, for spin-1/2 partons. Historically, the effect of the interference structure functions on the measured cross sections was parameterized as *constants* describing a possible $cos(\phi)$ and $cos(2\phi)$ dependence,

that were also shown to disappear in the asymptotic limit. Obviously, this assumption can not be correct at lower beam energies, where these interference structure functions can depend on all kinematical variables (x, Q^2, p_T, z).

Regardless, the holy grail of studies of this semi-inclusive process can easily be outlined, as the tagging of the type of coincident hadron gives access to the flavor of the struck quark via the correlation in flavor of the quark and the hadron. This is the advantage of semi-inclusive DIS (SIDIS), where not only the sum, but the individual parton distributions can be accesssed.

The latter is similarly true for so-called deep exclusive scattering (DES) experiments. Here, the flavor of the generalized parton distribution can be probed. For the case of pion electroproduction, the recently-developed theorems factorizing these processes in terms of handbag diagrams into a hard-scattering process and a soft process, anticipate a behavior $R = \sigma_L/\sigma_T \sim Q^2$, at a constant value of Bjorken x, in the asymptotic limit. Obviously, the DES process equals the limit $z \rightarrow 1$ of the SIDIS process. In addition, there are longstanding arguments on the contributions of $\rho \rightarrow \pi^+\pi^-$ production to the measured $(e, e'\pi^+)$ SIDIS rates. In view of the above, such contributions may very well have a different behavior of $R = \sigma_L/\sigma_T$ at large z (and non-asymptotic beam energies) than here-to-fore assumed.

Hence, to shed more light on the role of R in SIDIS seems appropriate. Knowledge on R is fundamental in its own right to better understand to what extent the electroproduced pions at 12-GeV beam energies are the direct fragmentation products of the struck partons, and has great practical implications on the analysis of SIDIS experiments.

II. THEORY AND MOTIVATION

A. Inclusive Scattering

For inclusive electron-nucleon scattering the differential cross section can, in the one-photon approximation, be written as:

$$\frac{d^2\sigma}{d\Omega_e dE'} = \sigma_{Mott}\{W_2(Q^2, W^2) + 2W_1(Q^2, W^2)tan^2(\theta/2)\}, \tag{1}$$

with σ_{Mott} the Mott cross section defined as

$$\sigma_{Mott} = \frac{\alpha^2 cos^2(\theta/2)}{4E^2 sin^4(\theta/2)} \tag{2}$$

and W_1 and W_2 the structure functions that contain information about the electromagnetic structure of the nucleon.

In the Bjorken limit, in which both Q^2 and $\nu \rightarrow \infty$, but x is fixed, the structure functions W_1 and W_2 were found to exhibit scaling. Therefore, it was convenient to introduce the dimensionless functions F_1 and F_2, defined by

$$F_1(x, Q^2) = MW_1(\nu, Q^2) \ , \tag{3}$$
$$F_2(x, Q^2) = \nu W_2(\nu, Q^2) \ . \tag{4}$$

In the quark-parton model these F_1 and F_2 structure functions are given in terms of parton distributions, $q(x)$ and $\bar{q}(x)$,

$$F_2(x) = 2xF_1(x) = x \sum_q e_q^2 \left(q(x) + \bar{q}(x)\right) \ , \tag{5}$$

where $q(x)$ is interpreted as the probability to find a quark of flavor q in the nucleon with light-cone momentum fraction x. Here, one can directly see that inclusive scattering can only probe the sum of, but not the individual, parton distributions.

The inclusive cross section can also be expressed in terms of σ_T and σ_L, the cross sections for the absorption of transverse and longitudinal photons, respectively. From this perspective, the ratio of longitudinal to transverse cross sections is expressed as

$$R \equiv \frac{\sigma_L}{\sigma_T} = \frac{F_2}{2xF_1}\left(1 + \frac{4M^2x^2}{Q^2}\right) - 1 \ . \tag{6}$$

Note that while the F_1 structure function is related only to the transverse virtual photon coupling, F_2 is a combination of both transverse and longitudinal couplings. For historical reasons, the world DIS data is expressed in terms of F_2 and R. For asymptotic energies, $R \to 1/Q^2 \to 0$, but for the case of kinematics accessible with a 12-GeV JLab, with Q^2 limited to ~ 3 GeV^2, R remains rather constant, to only drop $\sim 1/Q^2$ beyond. This can *e.g.* be seen in Fig. 1 [1]. Note that all DIS measurements of R on deuterium are up to now in excellent agreement with the data on hydrogen.

B. Semi-Inclusive Scattering

In the one-photon exchange approximation, the pion electroproduction cross section can in general be written as the product of a virtual photon flux (Γ) and a virtual photon cross section (evaluated in the laboratory frame),

$$\frac{d\sigma}{d\Omega_e dE_e d\Omega_\pi dM_x} = \Gamma \frac{d\sigma}{d\Omega_\pi dM_x} \ , \tag{7}$$

where M_x is the missing mass of the recoiling system, $M_x^2 = (q + P_A - p_\pi)^2$. The virtual photon flux is given by

$$\Gamma = \frac{\alpha}{2\pi^2}\frac{E_e'}{E_e}\frac{1}{Q^2}\frac{1}{1-\epsilon}\frac{W^2 - M^2}{2M} \ . \tag{8}$$

Here. ϵ is the virtual-photon polarization. The virtual-photon cross section can be written as

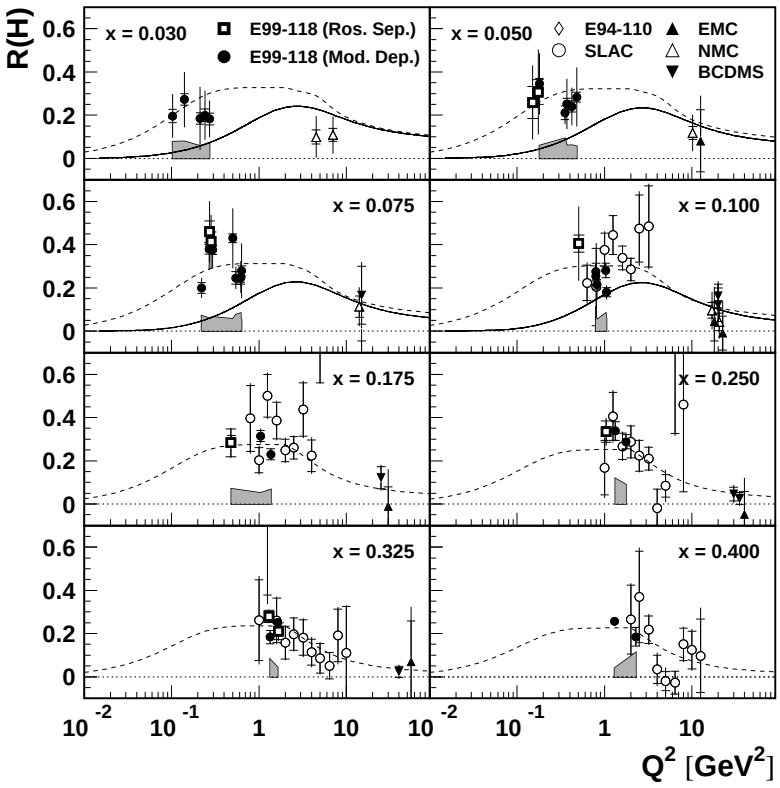

FIG. 1. Comparison of the values of R for hydrogen from the E99-118 experiment to the results of other experiments [1]. The dashed curves show a parameterization of the world's data for R also obeying current conservation for the limit $Q^2 \to 0$. The solid curves reflect the model developed in [2], based on a photon-gluon fusion mechanism suitably extrapolated into the region of low Q^2.

$$\frac{d\sigma}{d\Omega_\pi dM_x} = \frac{d\sigma_T}{d\Omega_\pi dM_x} + \epsilon\frac{d\sigma_L}{d\Omega_\pi dM_x} + \epsilon\frac{d\sigma_{TT}}{d\Omega_\pi dM_x}\cos 2\phi_{pq} + \sqrt{2\epsilon(1+\epsilon)}\frac{d\sigma_{LT}}{d\Omega_\pi dM_x}\cos\phi_{pq}\,, \tag{9}$$

where ϵ describes the longitudinal polarization of the virtual photon. In parallel kinematics, the interference terms (σ_{LT} and σ_{TT}) are small, and for complete ϕ ($= \phi_{pq}$) coverage integrate to zero. The cross sections can be parameterized in terms of four structure functions, W_L, W_T, W_{TT} and W_{LT}, that in general now depend on Q^2, W^2, z and p_T.

In the Bjorken limit, these formulas should simplify again, and can be more intuitively expressed in a quark-parton model. From perturbative QCD, there now will be factorization between the virtual photon–quark interaction and the subsequent quark hadronization,

$$\frac{\frac{d\sigma}{d\Omega_e dE_e dz dp_T^2 d\phi}}{\frac{d\sigma}{d\Omega_e dE_e}} = \frac{dN}{dz} b e^{-bp_T^2}\frac{1 + Acos(\phi) + Bcos(2\phi)}{2\pi}, \tag{10}$$

$$\frac{dN}{dz} \sim \sum_q e_q^2\; q(x,Q^2)\; D_{q\to\pi}(z,Q^2), \tag{11}$$

where the fragmentation function $D_{q\to\pi}(z,Q^2)$ gives the probability for a quark to evolve into a pion π detected with a fraction z of the quark (or virtual photon) energy, $z = E_\pi/\nu$. The transverse momentum p_T, z and the angle ϕ reflect the extra kinematical degree of freedom associated with the pion momentum, with b the average transverse momentum of the struck quark. At very high energies, the factors A and B (that in reality express the dependence on the two interference structure functions, and thus could in principle depend on Q^2, W^2, z and p_T again) become zero.

A consequence of this factorization is that the fragmentation function is independent of x, and the parton distribution function is independent of z. Both the parton distribution functions and the fragmentation functions, however, depend on Q^2 through logarithmic Q^2 evolution. The factorization in terms of a virtual photon-quark interaction and a subsequent quark hadronization implies the assumption that the electroproduced pions are indeed the fragmentation products of this virtual photon-quark interaction.

The above then indeed allows one to separate the subsequent processes by separation of the dependence on x and z. Further, tagging of the type of coincident hadron then could indeed give access to the flavor of the struck quark via the correlation in flavor of the quark and the hadron, as pictorially shown in Fig. 2.

At lower energies, it is not obvious that the pion electroproduction process factorizes in the same manner as in Eq. (11). Recently, a large data set of pion electroproduction from both hydrogen and deuterium targets has been obtained spanning the nucleon resonance region. These data conclusively showed the onset of quark-hadron duality in semi-inclusive $(e, e'\pi)$ processes, and the relation of this phenomenon to the high-energy factorization ansatz of subsequent electron-quark scattering and quark $\to$ pion production mechanisms. We have appended a nearly-final draft on the initial findings of this E00-108 experiment [3].

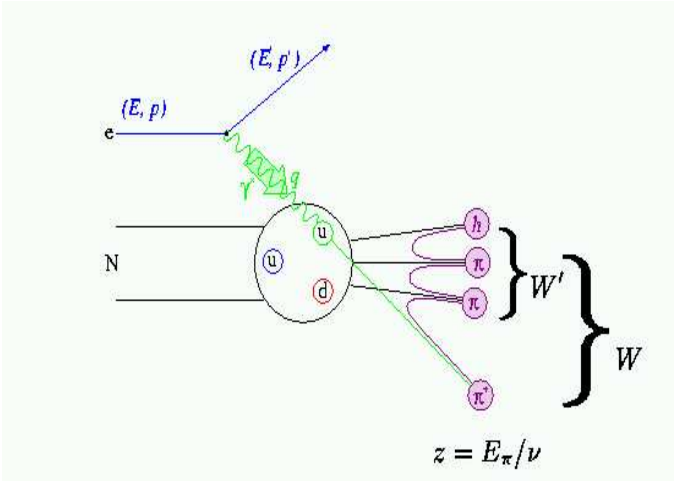

FIG. 2. Diagram showing the Semi-Inclusive DIS process. W' represents the missing mass M_X for the $(e, e'\pi)$ process.

The E00-108 ^{1,2}H(e,e$'\pi^{\pm}$)X cross sections as measured at $x = 0.32$ were compared with the results of a SIDIS simulation in Fig. 3, as a function of z. The general agreement between data and Monte Carlo is excellent for $z < 0.65$. Within the E00-108 kinematics ($p_T \sim 0$), M_x^2 is almost directly related to z, as $W'^2 \equiv M_x^2 = M_p^2 + Q^2(1/x - 1)(1 - z)$. Hence, the large "rise" in the data with respect to the simulation at $z > 0.8$ mainly reflects the $N - \Delta(1232)$ region. Indeed, if one considers a ^{1}H(e,e$'\pi^-$)X spectrum as function of missing mass of the residual system X, one sees only one prominent resonance region, the $N - \Delta$ region. Apparently, above $M_x^2 = 2.5$ GeV^2 or so, there are already sufficient resonances to render a spectrum mimicking the smooth z-dependence as expected from the Monte Carlo simulation following the factorization ansatz of Eq. (11). In the latter, we assumed $R_{SIDIS} = R_{DIS}$.

Note that events from diffractive ρ production were subtracted here. For this, we used PYTHIA to estimate the p(e,e$'\rho^{\circ}$)p cross section, with similar modifications as implemented by the HERMES collaboration [4,5].

Given the quantitative agreement between the measured low-energy data and the high-energy factorization ansatz of Eq. (11), using universal parton distribution and fragmentation functions as input, one would be tempted to conclude that quark-hadron duality also affects the long-range dynamics of confinement as given by the fragmentation process. Hence, even when one is at low energies, in a region where nucleon resonance (or hadronic) excitations are non-negligible, the fragmentation products seem to remain linked to the struck partons. It's exactly the latter idea that can far better be quantitatively tested in comparing the ratio R in semi-inclusive scattering to that of deep inelastic scattering.

As such, it is of prime importance to also map the behavior of R_{SIDIS} versus the transverse momentum p_T. One would anticipate that at low energies, the bahavior of

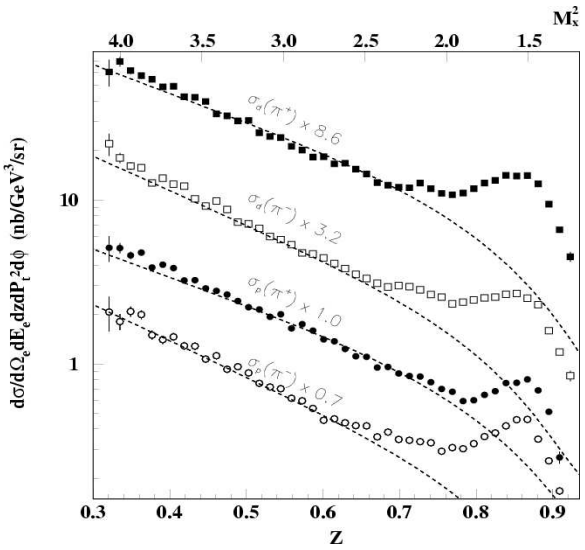

FIG. 3. The ^{1,2}H(e,e$'\pi^{\pm}$)X cross sections at $x = 0.32$ as a function of z in comparison with Monte Carlo simulations (dashed curves) starting from a fragmentation ansatz. The various cross sections have been multiplied as indicated for the purpose of plotting [3].

the p_T spectrum mimics the angular distributions of the nucleon resonance decays more, whereas at large p_T one reaches the hard scattering limit again. Hence, at large p_T R_{SIDIS} must anneal to R_{DIS} for consistency reasons.

C. Deep Exclusive Scattering

Over the last decade, QCD factorization theorems were derived for various deep inelastic exclusive processes [6–9]. These factorization theorems are intrinsically related to the access to Generalized Parton Distributions (GPD's), introduced by Ji and Radyushkin [10,11]. The discovery of these GPD's and their connection to certain totally exclusive cross sections has made it possible in principle to rigorously map out the complete nucleon wave functions themselves. The GPD's contain a wealth of information about the transverse momentum and angular momentum carried by the quarks in the proton. Presently, experimental access to such GPD's is amongst the highest priorities in intermediate energy nuclear/particle physics.

It is still uncertain at which Q^2 value one will reach the factorization regime, where the leading-order perturbative QCD domain fully applies for meson electroproduction. However, it is expected to be between $Q^2 = 5$ and 10 (GeV/c)^2.

The leading-twist perturbative QCD contribution in the case of hard meson electroproduction involves an additional one-gluon exchange. Due to helicity conservation, this implies that the QCD factorization theorems for this process expect a scaling behavior

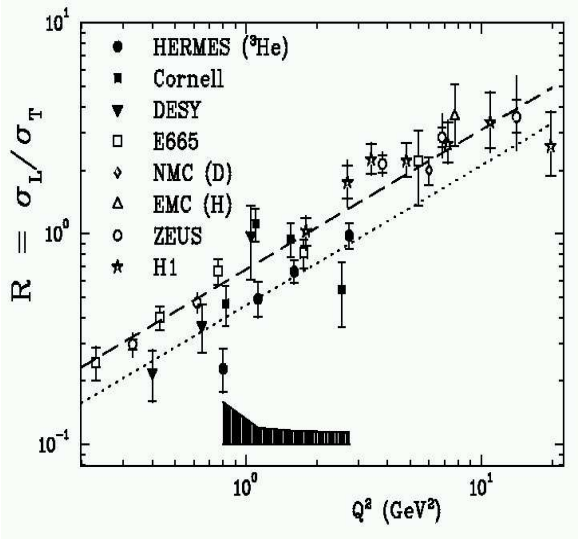

FIG. 4. The ratio $R = \sigma_L/\sigma_T$ for the $(e, e'\rho^\circ)$ process as a function of Q^2.

$R = \sigma_L/\sigma_T \sim Q^2$, at constant Bjorken x. This is in sharp contrast to the behavior expected for the SIDIS region!

First of all, this means that at asymptotic energies the behavior of R for $z < 1$ has disappeared like $1/Q^2$, whereas the ratio R is very large for $z = 1$. Surely, such a behavior is worth investigating at the Q^2 values accessible at a 12-GeV JLab, as a function of z. However, there is also, again, a practical implication. As mentioned earlier, events from $\rho \to \pi^+\pi^-$ production either contribute to the the SIDIS cross section, or are subtracted (the diffractive contribution).

The ratio $R = \sigma_L/\sigma_T$ in diffractive electroproduction of ρ° mesons has been measured, through angular distributions, quite extensively up to large Q^2. The results are displayed in Fig. 4, for a mixture of W values. It can be clearly seen that the data for this process indeed already show a rise with Q^2 of R, in a region where data for the SIDIS process are expected to exhibit a flat (at low Q^2) or $1/Q^2$ (at higher $Q^2 > 3$ GeV^2) behavior. This would definitely complicate any conclusions of a JLab 12-GeV SIDIS program at large z, as this will affect the amount of diffractive ρ production that needs to be subtracted from the SIDIS measurements at large z, at low energies.

D. The Inclusive-Exclusive Connection

The exclusive–inclusive connection in hadronic physics dates back to the early dates of deep inelastic scattering and the discussion of scaling laws in high energy processes. Bjorken & Kogut [12] articulated the correspondence relations by demanding the continuity of the dynamics as one goes from one (known) region of kinematics to another (which is unknown or poorly known). In analogy, in the correspondence principle in

quantum mechanics, the behavior of a quantum theory is connected with the known classical limit, which in turn leads to insights into the quantum theory itself.

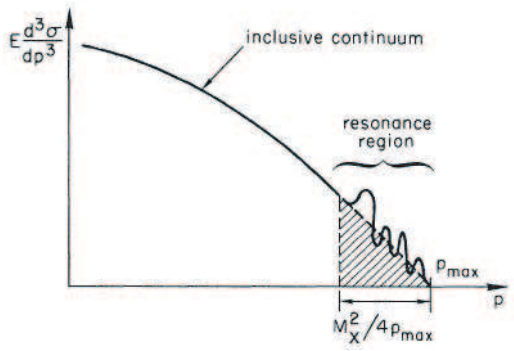

FIG. 5. Momentum spectrum of produced hadrons in the inclusive hadron production reaction $\gamma^* N \to MX$. From Ref. [12].

For two-body processes, such as $\gamma^* N \to MB$, the correspondence principle connects properties of exclusive (resonant) final states with inclusive particle spectra, described in terms of the differential cross section, $Ed^3\sigma/dp^3$, for the corresponding reaction $\gamma^* N \to MX$, where E and p are the energy and momentum of one of the observed final state particles. An illustration of a typical inclusive momentum spectrum for the observed particle M is shown in Fig. 5. As p increases, one steps from the inclusive continuum to the region dominated by resonances. The correspondence argument states that the magnitude of the resonance contribution to the cross section should be comparable to the continuum contribution extrapolated from high energy into the resonance region.

For inclusive electroproduction, it was used to derive the Drell-Yan–West relation between the asymptotic behavior of the elastic form factor and structure function in the $x \to 1$ limit. For our application, $\gamma^* N \to \pi X$, there must be an equivalent connection in the $z \to 1$ limit. However, the DES process is expected to be dominated by the longitudinal process in the asymptotic limit, whereas the SIDIS process follows the DIS process in the asymptotic limit, where the longitudinal contributions die off. The measurement of R as a function of z will inform us how the struck quark converts into the measured pion in these processes, by one hard-gluon exchange or a series of soft-gluon exchanges.

E. Motivation Summary

In summary, we will measure R in the SIDIS process, to

- Verify whether $R_{SIDIS} = R_{DIS}$.
- Check the z-dependence of R as one transitions from the semi-inclusive to the exclsuive region.
- Verify that R_{SIDIS} anneals to R_{DIS} at large p_T.

- Verify that R_{SIDIS} follows the expected Q^2 dependence of R_{DIS}.

The physics of interest is to what extent the struck quark indeeds fragments into the measured pion, even at lower beam energies, to study the long-range dynamics of confinement. In addition, we will study the connection between pion formation in semi-inclusive kinematics and the exclusive limit. Lastly, there are great practical advantages of these measurements for the general SIDIS program at a 12-GeV JLab, *e.g.*, for measurements of the light quark sea flavor asymmetry, a flavor decomposition of the nucleon spin at $x > 0.1$, and measurements of azimuthal asymmetries in SIDIS.

III. EXPERIMENT

Our goal will be the first thorough study of the ratio $R = \sigma_L/\sigma_T$ in SIDIS scattering. These measurements will provide direct input on the relation of the electroproduced pion with the struck quark, and provide a baseline understanding for the interpretation of SIDIS cross section measurements.

A. Experimental overview

The experiment will use the HMS and SHMS magnetic spectrometers for coincidence measurement of scattered electrons and pions from the semi-inclusive electroproduction reaction $(e, e'\pi^{\pm})$X. The role of HMS and SHMS may be reversed in some kinematics, but in general SHMS, with its most forward angle of 5.5°, will detect the electroproduced pions.

We intend to perform all measurements on a hydrogen target, apart from the necessary Al "dummy" measurements for target wall subtraction, and one series of measurements on a deuterium target to validate $R^H_{SIDIS} = R^D_{SIDIS}$, in a kinematics region overlapping with another SIDIS experiments intending to do a flavor decomposition.

The experiment will use beam energies of 6.6, 8.8, and 11.0 GeV to accomplish the Rosenbluth separations. For each Rosenbluth separation, we will use fixed values of x, Q^2, z, and p_T^2. The series of measurements will provide scans in z, up to the exclusive limit, p_T^2, and Q^2. The largest fraction of the beam time will be at the lowest beam energy, to provide the lowest value of the virtual photon polarization, ϵ. In general, the range of ϵ for the Rosenbluth separations is ~ 0.5. We expect systematic uncertainties very similar to those of previous inclusive measurements of R_{DIS}.

We will use the simultaneously measured inclusive cross sections to determine $R = \sigma_L/\sigma_T$ for inclusive (e,e'x) DIS and compare with the SIDIS data. We may alternatively use these data for systematics control.

B. Spectrometer system

In this experiment, we will make coincidence measurements between pions and electrons. Single arm rates up to a level of 1 MHz and good pion/electron, pion/kaon,

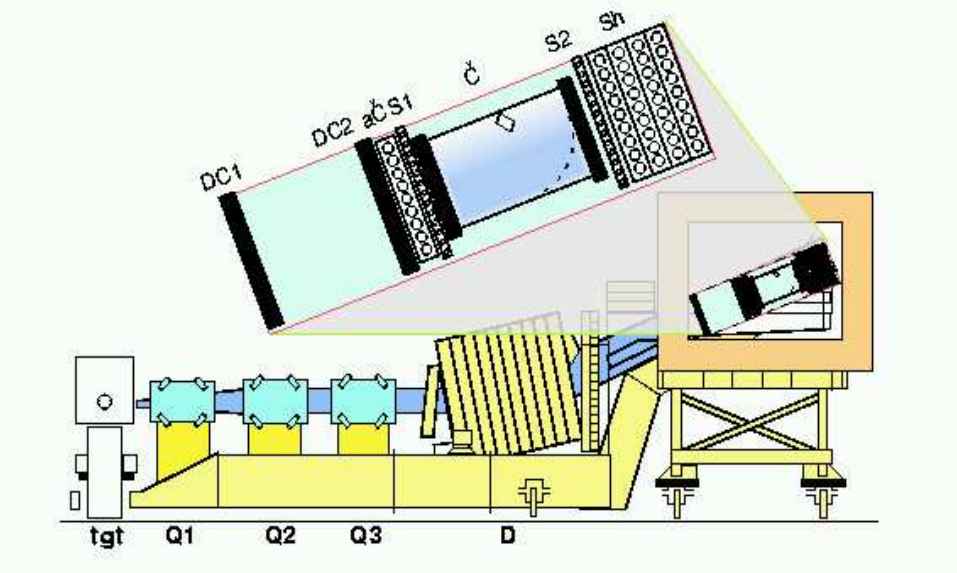

FIG. 6. Block Diagram of the HMS and its detector package.

pion/kaon/proton separation capabilities have routinely been achieved in Hall C for many years in the HMS/SOS combination. *E.g.*, the current detector stack of the HMS has been shown to easily achieve e^-/π^- to $\sim 10^3$, with 98% efficiency. The SHMS design of the optics and the detector system is essentially a clone of the HMS design, so we expect very similar properties.

Together, the capability of HMS and SHMS will allow us without any problem to access the momentum and angular ranges of scattered electrons and electro-produced mesons in the kinematic range of our interest:

HMS (see Fig. 6) has a QQQD optics design. HMS has been used in many experiments which require good particle identification, high rate capability and, especially, accurate knowledge of the acceptance. The HMS solid angle is $\sim$ 6 msr, with a momentum acceptance of $\pm$10.0%. The minimum angle relative to the beam is $\sim$10.5°, with a maximum momentum of up to 7.3 GeV/c. The HMS detector package consists of two drift chambers for track reconstruction, two sets of x-y scintillator hodoscopes for triggering and time-of-flight studies, a gas Cerenkov counter, an Aerogel detector and a Lead-glass calorimeters for particle identification.

SHMS has a (D)QQQD design, where the first dipole is a small horizontal prebender and the remainder is a conventional QQQD vertical bend design, very similar to the HMS design. The SHMS design is optimized to reach the highest momentum settings (up to 11 GeV/c) and the smallest scattering angles (down to 5.5°). The SHMS acceptance is projected to be about 4 msr, with a momentum acceptance of -15% to +20%. The detector package (see Fig. 7) is very similar as the HMS detector package. It will contain a noble-gas Cherenkov at sub-atmospheric pressure (not used in this experiment), two SOS-type chambers for track reconstruction, an x-y scintillator hodoscope

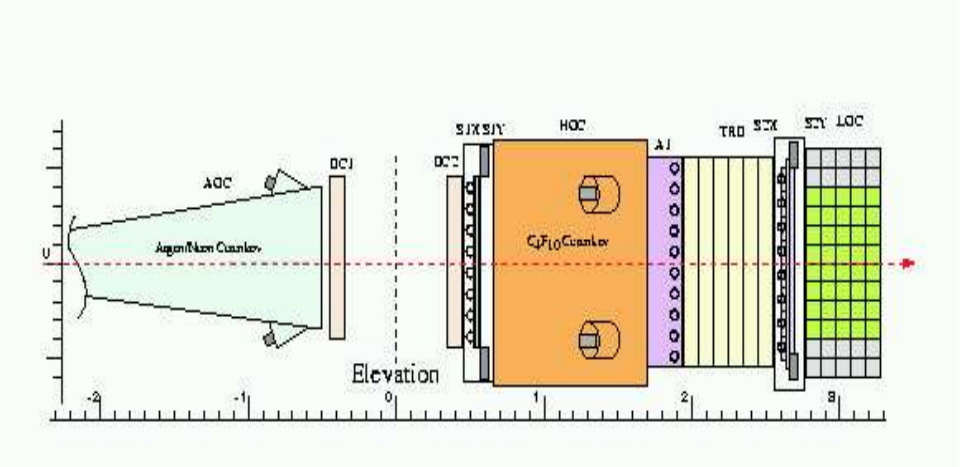

FIG. 7. Block diagram of the detector package of the SHMS, highlighting the similarities between HMS and SHMS. The only difference is in the dedicated space for additional particle identification detectors, in this block diagram filled with an Aerogel detector and a TRD detector. The latter are not part of the SHMS Base Equipment package. However, it is anticipated that an Aerogel detector, essentially a clone of the HMS Aerogel detector, will be constructed early in the 12-GeV operations phase.

for timing/triggering, a heavy gas Cerenkov, an x-y quartz Cerenkov hodoscope for timing/triggering, and a Lead-glass shower counter. There is additional space for dedicated particle identification detectors such as Aerogel Cherenkovs.

C. The Liquid Target

We have assumed 10 cm long cryogenic Hydrogen and Deuterium targets in our beam time estimates. The default target lengths used in Hall C are 4 cm and 15 cm long. We could in principle do the experiments with 15 cm long targets, but it is good practice to do precision Rosenbluth separations with targets that closely mimic point-like targets for the spectrometers.

The target density will be monitored by pressure and temperature measurements. At the assumed beam current of $\sim 50\mu$A we expect negligible change in target densities, with the fast raster systems already in place: We expect less than 1% density changes at 100 μA, for a raster size of 2×2 mm^2.

D. Electronics and DAQ

Because of moderate pion to electron ratios (about 100 to 1) for some of the kinematic settings, we will require the events of interest to pass some loose particle identification cuts before generating a trigger. In order to have a high efficiency for electrons, a

trigger will be accepted as a true electron if either the Cherenkov has fired or if the electromagnetic calorimeter will have a large enough signal. This will allow high electron efficiency even if one of the two detectors will have a low efficiency.

The electron trigger (ELREAL) will thus have two components: Electron High (ELHI) and Electron Low (ELLO). ELHI will require a high calorimeter signal, but no gas Cerenkov information, and will be composed of a high signal in the "preshower" (PRHI) and a low signal in the full calorimeter (SHLO), in coincidence with scintillator signal (SCIN). Note that the "preshower" for the HMS is simply the first layer of the calorimeter. ELLO will require the Cherenkov signal.

The pion trigger (PION) will require only a standard three-out-of-four (3/4) coincidence of the x-y hodoscopes (SCIN), vetoed by a Cherenkov signal (CER). The final coincidence trigger (COIN) will be a combinetion of electron (ELREAL) and pion (PION) triggers.

The DAQ will predominantly run in 'coin' mode to maintain the maximum capability for data acquisition of coincidence events. In addition, single-arm triggers will be accumulated with low priority, to take inclusive (e,e') and (e,h) data. To avoid significant dead-time during high-rate runs and keep the DAQ efficiency for coincidence events high, the single-arm triggers will be prescaled.

For precision experiments with the HMS, its rate has typically been limited to 0.5 MHz to obtain good confidence in the tracking efficiency. This is due to a combination of the gate width for the readout of the wire chamber TDC's, and the HMS chambers not providing sufficient "y" measurements. It is fully anticipated that we can obtain good knowledge of the tracking efficiencies with higher rates at 12 GeV, using the planned multi-hit TDC's and the SOS-type chambers.

E. Particle Identification

The main focus of the experiment will be on pion production. For PID, we will combine functions of the hodoscope Time-Of-Flight (TOF) detectors, Gas Cherenkov and Aerogel Cherenkov detectors, and shower counters in each spectrometer arm. In addition, in the off-line analysis, we will use a cut on the coincidence timing between electron and hadron. Regular cuts on kinematic variables, such as vertex, collimator, spectrometer acceptance, etc., will also be used to reduce any background.

The Hall C HMS has been used in many experiments which required good particle identification and accurate knowledge of the acceptance. The HMS angular and momentum acceptance are $\sim$6 msr and $\pm$ 10 %. The gas Cerenkov in the HMS can be filled with either C_4F_{10} or CO_2, at a pressure as low as 0.4 atm and as high as $\sim$ 3 atm. We will choose the pressure and gas to optimize for π/e selection for our kinematic range.

The lead-glass Shower Counter in HMS consists of 4 layers, each with a thickness of about four radiation lengths. Total energy deposition and information about the electromagnetic shower development (energy from each layer) could be used for a more effective separation of electrons from hadrons.

The energy resolution of the calorimeter can be approximated as:

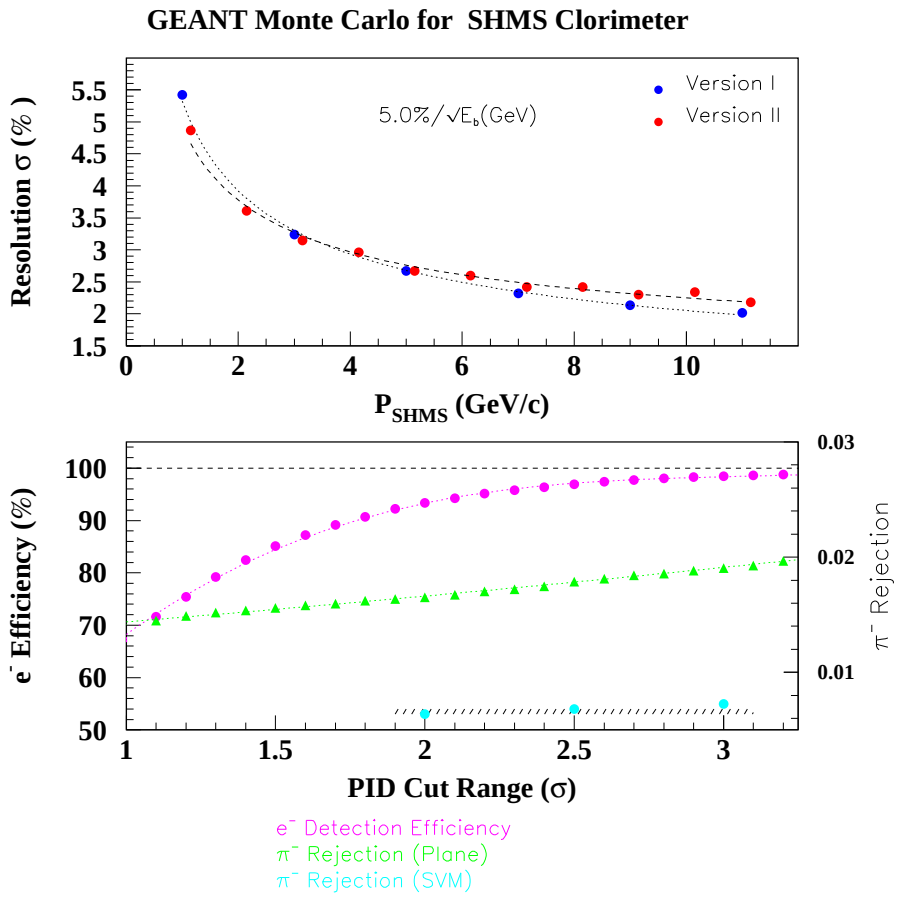

FIG. 8. GEANT Simulation for SHMS Calorimeter

$$\sigma \simeq 6.1/\sqrt{E}. \tag{12}$$

This gives $\sim$ 7 % at energy 1 GeV. The electron detection efficiency ϵ has been shown to be $\geq$ 99.5%. Based on data from previous experiments, a pion rejection factor of 1,000:1 can be achieved at E $\geq$ 2.0 GeV with a 98 % electron detection efficiency.

It is proposed to construct for SHMS a shower detector similar to the HERMES calorimeter. Such a calorimeter will be a combination of Shower and Preshower with a total thickness of about 20 radiation lengths. Based on the detailed simulation, performed by the Yerevan group, and existing data we expect this calorimeter to have more than 98% electron detection efficiency, good energy resolution and high electron-pion rejection capability (see Fig. 8)

The Yerevan group, in collaboration with Hall C staff, recently built and commissioned an HMS Aerogel detector [13], already successfully used in a series of Hall C experiments for pion-proton separation (see Fig. 9). It is anticipated that a similar detector will be built for SHMS during the initial 12-GeV operations phase. For the proposed experiment, we do not require an Aerogel Cherenkov detector, although it will be useful for kaon identification.

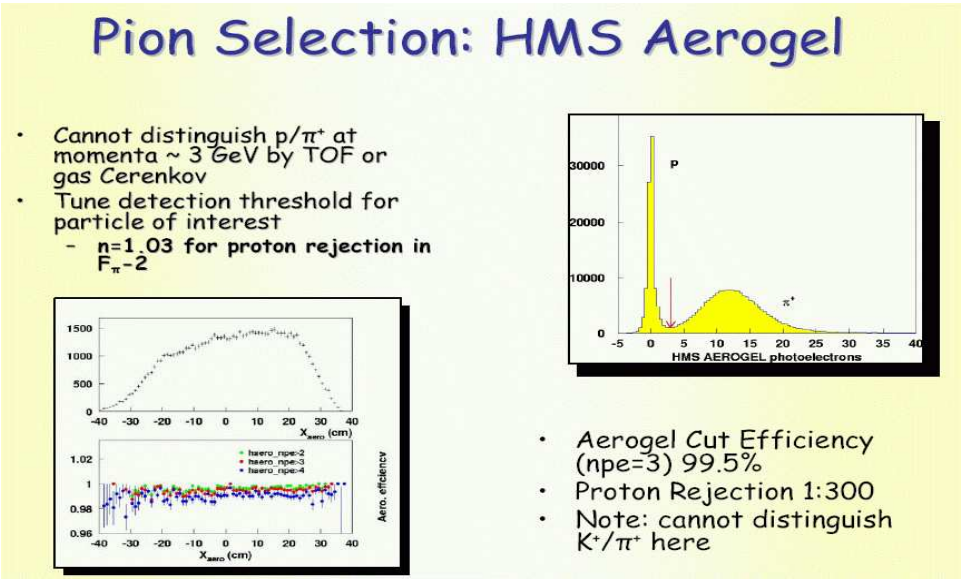

FIG. 9. The Pion-Proton selection capability of the HMS Aerogel detector

It is proposed to construct a similar as in HMS threshold Cerenkov detector for SHMS, using heavy per-fluorocarbon gas C_4F_{10}. We expect that with optimal pressure of gas, we have a clean way for electron identification.

Adding atmospheric pressure Cerenkov in place of the last section of vacuum pipe (upstream of the first wire chamber) can provide additional PID capability. This device is using a Ne-Ar mixture at atmospheric pressure. Its index can be tuned to enhance

the electron-pion discrimination. We don't anticipate needing this detector, but it could provide a backup solution.

The second hodoscope plane in SHMS will consist of a ∼2 cm thick quartz Cerenkov radiator elements. A quartz Cerenkov operated at a threshold of 100 photoelectrons could be essential 100 % efficient and blind to low energy backgrounds, resulting in a much cleaner trigger.

Based on all detectors capability, the expected π^-/e^- separation can be achieved up to 10^-3-10^-4 for a given electron efficiency of $\geq 99\%$ each, for the electron spectrometer. When the HMS (or the SHMS) will be used for pion detection, the shower counter will also be used for e^- (e^+) rejection. In this case, an 100:1 electron rejection can be achieved. The total electron rejection (gas Cerenkov + Calorimeter), finally, is expected to be on the level of 1,000:1 with a pion detection efficiency better than 99.5 %.

The coincidence timing resolution is expected to be ∼200 ps. In this case a 3 σ coincidence window (1.2 ns) will be used to select real events.

IV. PROPOSED MEASUREMENTS

A. Choice of Kinematics

We propose to perform the first complete study of measurements of $R = \sigma_L/\sigma_T$ in semi-inclusive deep inelastic scattering. Based upon the discussion in the Theory and Motivation Section, we propose the following:

- Map R as a function of z at $x = 0.20$ and $Q^2 = 2.00$ GeV^2, for both hydrogen and deuterium targets. This kinematics is chosen for compatibility reasons with the expected flavor decomposition program at a 12-GeV JLab. Especially, we would like to verify in at least one case that $R^H_{SIDIS} = R^D_{SIDIS}$. The chosen kinematics are given in Table I.

- Map R^H as a function of z at $x = 0.40$ and $Q^2 = 4.00$ GeV^2. Note that by keeping the ratio Q^2/x fixed, we keep the virtual-photon momentum nearly fixed. The z values are then chosen such that the full SHMS momentum acceptance allows for overlap in z. At this value of Q^2, it is expected that $R_{DES} > R_{SIDIS}$. The chosen kinematics are given in Table II.

- Map R_H as a function of p_T^2 at $x = 0.30$ and $Q^2 = 3.00$ GeV^2. The (x, Q^2) combination is chosen to allow this scan within a reasonable amount of beam time. A lower value of (x, Q^2) would preclude measurements at both sides (left/right) of the virtual-photon direction. The kinematics are given in Table III.

- Add two additional kinematics to allow a map of R^H ranging from $Q^2 = 1.5$ to 5.0 GeV^2. The kinematics are given in Table IV.

TABLE I. L/T Separations as a function of z at (x, Q^2) = (0.20,2.00)

x	Q^2 (GeV^2)	W^2 (GeV^2)	z	W'^2 (GeV^2)	E' (GeV)	θ_e (deg)	q_γ (GeV)	θ_γ (deg)	ϵ	Eo (GeV)	R_{DIS}
0.20	2.00	8.88	0.30	6.48	1.271	28.26	5.513	6.27	0.34	6.6	0.27
			0.30	6.48	3.471	14.70	5.513	9.19	0.66	8.8	0.27
			0.30	6.48	5.671	10.27	5.513	10.57	0.80	11.0	0.27
0.20	2.00	8.88	0.40	5.68	1.271	28.26	5.513	6.27	0.34	6.6	0.27
			0.40	5.68	3.471	14.70	5.513	9.19	0.66	8.8	0.27
			0.40	5.68	5.671	10.27	5.513	10.57	0.80	11.0	0.27
0.20	2.00	8.88	0.50	4.88	1.271	28.26	5.513	6.27	0.34	6.6	0.27
			0.50	4.88	3.471	14.70	5.513	9.19	0.66	8.8	0.27
			0.50	4.88	5.671	10.27	5.513	10.57	0.80	11.0	0.27
0.20	2.00	8.88	0.65	3.68	1.271	28.26	5.513	6.27	0.34	6.6	0.27
			0.65	3.68	3.471	14.70	5.513	9.19	0.66	8.8	0.27
			0.65	3.68	5.671	10.27	5.513	10.57	0.80	11.0	0.27
0.20	2.00	8.88	0.85	2.08	1.271	28.26	5.513	6.27	0.34	6.6	0.27
			0.85	2.08	3.471	14.70	5.513	9.19	0.66	8.8	0.27
			0.85	2.08	5.671	10.27	5.513	10.57	0.80	11.0	0.27

TABLE II. L/T Separations as a function of z at $(x, Q^2) = (0.40,4.00)$

x	Q^2 (GeV^2)	W^2 (GeV^2)	z	W'^2 (GeV^2)	E' (GeV)	θ_e (deg)	q_γ (GeV)	θ_γ (deg)	ϵ	Eo (GeV)	R_{DIS}
0.40	4.00	6.88	0.30	5.08	1.271	40.40	5.692	8.32	0.31	6.6	0.19
			0.30	5.08	3.471	20.85	5.692	12.54	0.65	8.8	0.19
			0.30	5.08	5.671	14.55	5.692	14.49	0.79	11.0	0.19
0.40	4.00	6.88	0.40	4.48	1.271	40.40	5.692	8.32	0.31	6.6	0.19
			0.40	4.48	3.471	20.85	5.692	12.54	0.65	8.8	0.19
			0.40	4.48	5.671	14.55	5.692	14.49	0.79	11.0	0.19
0.40	4.00	6.88	0.50	3.88	1.271	40.40	5.692	8.32	0.31	6.6	0.19
			0.50	3.88	3.471	20.85	5.692	12.54	0.65	8.8	0.19
			0.50	3.88	5.671	14.55	5.692	14.49	0.79	11.0	0.19
0.40	4.00	6.88	0.65	2.98	1.271	40.40	5.692	8.32	0.31	6.6	0.19
			0.65	2.98	3.471	20.85	5.692	12.54	0.65	8.8	0.19
			0.65	2.98	5.671	14.55	5.692	14.49	0.79	11.0	0.19
0.40	4.00	6.88	0.85	1.78	1.271	40.40	5.692	8.32	0.31	6.6	0.19
			0.85	1.78	3.471	20.85	5.692	12.54	0.65	8.8	0.19
			0.85	1.78	5.671	14.55	5.692	14.49	0.79	11.0	0.19

TABLE III. L/T Separations as a function of p_T^2 at $(x, Q^2) = (0.30,3.00)$

x	Q^2 (GeV^2)	W^2 (GeV^2)	z	W'^2 (GeV^2)	E' (GeV)	θ_e (deg)	q_γ (GeV)	θ_γ (deg)	ϵ	Eo (GeV)	R_{DIS}	θ_{pq} (deg)
0.30	3.00	7.88	0.50	4.380	1.271	34.80	5.603	7.44	0.33	6.6	0.19	-2.0
			0.50	4.380	3.471	18.03	5.603	11.05	0.66	8.8		
			0.50	4.380	5.671	12.59	5.603	12.75	0.80	11.0		
0.30	3.00	7.88	0.50	4.380	1.271	34.80	5.603	7.44	0.33	6.6	0.19	0.0
			0.50	4.380	3.471	18.03	5.603	11.05	0.66	8.8		
			0.50	4.380	5.671	12.59	5.603	12.75	0.80	11.0		
0.30	3.00	7.88	0.50	4.380	1.271	34.80	5.603	7.44	0.33	6.6	0.19	5.0
			0.50	4.380	3.471	18.03	5.603	11.05	0.66	8.8		
			0.50	4.380	5.671	12.59	5.603	12.75	0.80	11.0		
0.30	3.00	7.88	0.50	4.380	1.271	34.80	5.603	7.44	0.33	6.6	0.19	10.0
			0.50	4.380	3.471	18.03	5.603	11.05	0.66	8.8		
			0.50	4.380	5.671	12.59	5.603	12.75	0.80	11.0		
0.30	3.00	7.88	0.50	4.380	1.271	34.80	5.603	7.44	0.33	6.6	0.19	15.0
			0.50	4.380	3.471	18.03	5.603	11.05	0.66	8.8		
			0.50	4.380	5.671	12.59	5.603	12.75	0.80	11.0		
0.30	3.00	7.88	0.50	4.380	1.271	34.80	5.603	7.44	0.33	6.6	0.19	20.0
			0.50	4.380	3.471	18.03	5.603	11.05	0.66	8.8		
			0.50	4.380	5.671	12.59	5.603	12.75	0.80	11.0		

TABLE IV. Additional L/T Separations as a function of Q^2 at variable (x, Q^2).

x	Q^2 (GeV^2)	W^2 (GeV^2)	z	W'^2 (GeV^2)	E' (GeV)	θ_e (deg)	q_γ (GeV)	θ_γ (deg)	ϵ	Eo (GeV)	R_{DIS}
0.15	1.50	9.38	0.50	5.130	1.271	24.41	5.468	5.51	0.35	6.6	0.35
			0.50	5.130	3.471	12.72	5.468	8.04	0.67	8.8	0.35
0.50	5.00	5.88	0.50	3.380	1.271	45.41	5.779	9.01	0.30	6.6	0.12
			0.50	3.380	3.471	23.34	5.779	13.77	0.64	8.8	0.12
			0.50	3.380	5.671	16.28	5.779	15.96	0.79	11.0	0.12

In all cases, we have made sure that the laboratory angle of SHMS is at least 5.5°, and the laboratory angle of HMS at least 10.5°. The range in ϵ is optimized for the Rosenbluth separations, and is typical ~ 0.5. The spectrometer momentum settings are well within the allowable ranges for the HMS and SHMS.

B. Singles Rate Estimates

The DIS (e,e′) rates were calculated using the NMC fits for the structure functions F_1 and F_2. The singles e^- rates were calculated for a Hydrogen target. The singles pion, kaon, and proton rates were estimated using parametrizations of SLAC data of Wiser *et al.* [14], also for a Hydrogen target. For the Deuterium target we will simply scale the beam intensity to keep the singles rates on the same level, which will minimize the systematic errors in the tracking efficiency.

We simply took a solid angle of 4 msr and a momentum acceptance of 30% for the singles rate estimates, which is a reasonable compromise between the HMS and SHMS acceptances. This was done for the sake of simplicity to calculate all singles rates, as the roles of the spectrometers will be reversed in various kinematics. We assumed a beam current of 50 μA.

The singles rates in the electron arm, under the assumptions sketched above, are given in Table V, whereas the singles rates in the hadron arm are given in Table VI.

We did also consider the background due to pair production. For electron-proton (deuteron) scattering there is a significant probability to produce neutral pions in the target, that can then, after decay, produce an electron-positron pair. Similarly, the Bethe-Heitler process can produce an electron-positron pair. Based on detailed studies in Halls B and C on such backgrounds, using a variety of nuclear targets, scattering angles, and spectrometer momenta, this background is considered insubstantial for the kinematics of interest. This is further substantiated with a 6-GeV test measurement in Hall C, where positrons were detected in SOS in coincidence with pions in HMS. Here, the background originating from π^0 production and its subsequent decay into two photons and then electron-positron pairs, was found to be negligible.

C. Coincidence Rate Estimates

We have added the possibility of semi-inclusive pion electroproduction to the general Hall C Monte Carlo package SIMC, following the high-energy expectation of Eq. (11). We used the CTEQ5 next-to-leading-order (NLO) parton distribution functions to parameterize $q(x, Q^2)$ [15], and the fragmentation function parameterization for $D^+_{q\to\pi}(z, Q^2) + D^-_{q\to\pi}(z, Q^2)$, with D^+ (D^-) the favored (unfavored) fragmentation function, from Binnewies *et al.* [16]. The remaining unknowns are the ratio of D^-/D^+, the slope b of the p_T dependence, and the parameters A and B describing the ϕ dependence.

Both the D^-/D^+ ratio [17] and the b-value [4] were taken from HERMES analyses ($b \approx 4.66$). We assumed the parameters A and B to be zero for the rate estimates, which

TABLE V. Single Rates in Electron Arm

x	Q^2 (GeV^2)	z	θ_{pq} (deg)	E (GeV)	E' (GeV)	θ_e (deg)	e^- (kHz)	π^- (kHz)	K^- (kHz)	π/e	I_{beam} (μA)
0.20	2.0	0.30	0.	6.6	1.3	28.3	0.5	63.0	2.2	130.5	25.
				8.8	3.5	14.7	5.6	25.2	1.9	4.5	25.
				11.0	5.7	10.3	20.9	14.0	1.4	0.7	25.
0.20	2.0	0.40	0.	6.6	1.3	28.3	0.5	63.0	2.2	130.5	25.
				8.8	3.5	14.7	5.6	25.2	1.9	4.5	25.
				11.0	5.7	10.3	20.9	14.0	1.4	0.7	25.
0.20	2.0	0.50	0.	6.6	1.3	28.3	0.5	63.0	2.2	130.5	25.
				8.8	3.5	14.7	5.6	25.2	1.9	4.5	25.
				11.0	5.7	10.3	20.9	14.0	1.4	0.7	25.
0.20	2.0	0.65	0.	6.6	1.3	28.3	0.5	63.0	2.2	130.5	25.
				8.8	3.5	14.7	5.6	25.2	1.9	4.5	25.
				11.0	5.7	10.3	20.9	14.0	1.4	0.7	25.
0.20	2.0	0.85	0.	6.6	1.3	28.3	1.0	126.0	4.4	130.5	50.
				8.8	3.5	14.7	11.2	50.4	3.8	4.5	50.
				11.0	5.7	10.3	41.8	28.0	2.8	0.7	50.
0.40	4.0	0.30	0.	6.6	1.3	40.4	0.1	6.8	0.2	91.4	25.
				8.8	3.5	20.8	0.9	1.4	0.1	1.6	25.
				11.0	5.7	14.5	6.4	1.2	0.1	0.2	50.
0.40	4.0	0.40	0.	6.6	1.3	40.4	0.1	6.8	0.2	91.4	25.
				8.8	3.5	20.8	1.7	2.8	0.2	1.6	50.
				11.0	5.7	14.5	6.4	1.2	0.1	0.2	50.
0.40	4.0	0.50	0.	6.6	1.3	40.4	0.1	13.6	0.3	91.4	50.
				8.8	3.5	20.8	1.7	2.8	0.2	1.6	50.
				11.0	5.7	14.5	6.4	1.2	0.1	0.2	50.
0.40	4.0	0.65	0.	6.6	1.3	40.4	0.1	13.6	0.3	91.4	50.
				8.8	3.5	20.8	1.7	2.8	0.2	1.6	50.
				11.0	5.7	14.5	6.4	1.2	0.1	0.2	50.
0.40	4.0	0.85	0.	6.6	1.3	40.4	0.1	13.6	0.3	91.4	50.
				8.8	3.5	20.8	1.7	2.8	0.2	1.6	50.
				11.0	5.7	14.5	6.4	1.2	0.1	0.2	50.
0.15	1.5	0.50	0.	6.6	1.3	24.4	0.6	80.3	2.9	136.1	15.
				8.8	3.5	12.7	6.7	39.0	2.9	5.7	15.
				11.0	5.7	8.9	25.6	23.5	2.2	0.9	15.
0.50	5.0	0.50	0.	6.6	1.3	45.4	0.1	4.9	0.1	78.9	50.
				8.8	3.5	23.3	0.7	0.8	0.0	1.1	50.
				11.0	5.7	16.3	2.7	0.3	0.0	0.1	50.
0.30	3.0	0.50	-2.	6.6	1.3	34.8	0.2	19.7	0.6	109.6	25.
				8.8	3.5	18.0	2.1	5.6	0.4	2.7	25.
				11.0	5.7	12.6	15.5	5.4	0.5	0.4	50.
0.30	3.0	0.50	5.	6.6	1.3	34.8	0.4	39.4	1.1	109.6	50.
				8.8	3.5	18.0	4.2	11.2	0.8	2.7	50.
				11.0	5.7	12.6	15.5	5.4	0.5	0.4	50.
0.30	3.0	0.50	10.	6.6	1.3	34.8	0.4	39.4	1.1	109.6	50.
				8.8	3.5	18.0	4.2	11.2	0.8	2.7	50.
				11.0	5.7	12.6	15.5	5.4	0.5	0.4	50.
0.30	3.0	0.50	15.	6.6	1.3	34.8	0.4	39.4	1.1	109.6	50.
				8.8	3.5	18.0	4.2	11.2	0.8	2.7	50.
				11.0	5.7	12.6	15.5	5.4	0.5	0.4	50.
0.30	3.0	0.50	20.	6.6	1.3	34.8	0.4	39.4	1.1	109.6	50.
				8.8	3.5	18.0	4.2	11.2	0.8	2.7	50.
				11.0	5.7	12.6	15.5	5.4	0.5	0.4	50.

TABLE VI. Single Rates in Hadron Arm

x	Q^2 (GeV^2)	z	θ_{pq} (deg)	E (GeV)	P_π (GeV)	θ_π (deg)	e^- kHz	π^- kHz	K^- kHz	π/e	I_{beam} (μA)
0.20	2.0	0.30	0.	6.6	1.7	6.3	64.5	1401.	41.	21.7	25.
				8.8	1.7	9.2	15.9	1132.4	43.8	71.4	25.
				11.0	1.7	10.6	6.7	1048.1	45.6	157.6	25.
0.20	2.0	0.40	0.	6.6	2.2	6.3	108.9	1076.6	35.4	9.9	25.
				8.8	2.2	9.2	20.8	791.4	37.4	37.9	25.
				11.0	2.2	10.6	8.1	707.3	38.6	87.3	25.
0.20	2.0	0.50	0.	6.6	2.8	6.3	165.8	728.2	25.8	4.4	25.
				8.8	2.8	9.2	26.3	494.7	27.2	18.8	25.
				11.0	2.8	10.6	9.5	429.7	28.0	45.1	25.
0.20	2.0	0.65	0.	6.6	3.6	6.3	295.2	334.6	12.0	1.1	25.
				8.8	3.6	9.2	36.1	210.6	13.6	5.8	25.
				11.0	3.6	10.6	11.7	178.3	14.1	15.1	25.
0.20	2.0	0.85	0.	6.6	4.7	6.3	1330.4	160.6	4.1	0.1	50.
				8.8	4.7	9.2	108.5	107.0	7.4	1.0	50.
				11.0	4.7	10.6	30.4	91.5	8.6	3.0	50.
0.40	4.0	0.30	0.	6.6	1.7	8.3	38.0	997.8	33.3	26.3	25.
				8.8	1.7	12.5	6.1	606.	27.6	98.4	25.
				11.0	1.7	14.5	4.6	979.2	50.3	212.4	50.
0.40	4.0	0.40	0.	6.6	2.3	8.3	56.8	651.6	25.3	11.5	25.
				8.8	2.3	12.5	15.2	654.2	37.1	42.9	50.
				11.0	2.3	14.5	5.3	488.2	31.8	92.3	50.
0.40	4.0	0.50	0.	6.6	2.8	8.3	161.7	745.0	31.4	4.6	50.
				8.8	2.8	12.5	18.3	314.1	20.7	17.2	50.
				11.0	2.8	14.5	5.9	217.9	16.8	36.8	50.
0.40	4.0	0.65	0.	6.6	3.7	8.3	270.6	260.9	10.9	1.0	50.
				8.8	3.7	12.5	23.4	88.4	6.6	3.8	50.
				11.0	3.7	14.5	6.8	55.9	5.1	8.3	50.
0.40	4.0	0.85	0.	6.6	4.8	8.3	565.5	39.5	0.9	0.1	50.
				8.8	4.8	12.5	30.4	12.0	0.9	0.4	50.
				11.0	4.8	14.5	7.5	7.1	0.7	1.0	50.
0.15	1.5	0.50	0.	6.6	2.7	5.5	144.3	601.7	19.9	4.2	15.
				8.8	2.7	8.0	26.7	469.4	23.7	17.6	15.
				11.0	2.7	9.2	10.1	435.3	26.1	43.1	15.
0.50	5.0	0.50	0.	6.6	2.9	9.0	129.7	573.4	25.3	4.4	50.
				8.8	2.9	13.8	12.9	194.3	13.4	15.0	50.
				11.0	2.9	16.0	4.0	21.8	9.8	30.4	50.
0.30	3.0	0.50	-2.	6.6	2.8	5.4	80.0	886.6	29.1	11.0	25.
				8.8	2.8	9.1	9.6	488.5	27.0	50.4	25.
				11.0	2.8	10.7	7.2	791.2	52.5	109.9	50.
0.30	3.0	0.50	5.	6.6	2.8	12.4	15.2	218.1	11.0	14.3	50.
				8.8	2.8	16.1	2.8	100.7	7.1	36.0	50.
				11.0	2.8	17.7	1.1	77.3	6.1	70.2	50.
0.30	3.0	0.50	10.	6.6	2.8	17.4	4.2	38.1	1.9	9.1	50.
				8.8	2.8	21.1	0.8	16.1	1.1	18.8	50.
				11.0	2.8	22.7	0.3	12.0	0.9	42.7	50.
0.30	3.0	0.50	15.	6.6	2.8	22.4	1.3	5.4	0.2	4.6	50.
				8.8	2.8	26.1	0.2	2.1	0.1	18.8	50.
				11.0	2.8	27.7	0.0	1.5	0.1	42.7	50.
0.30	3.0	0.50	20.	6.6	2.8	27.4	0.4	0.6	0.0	4.6	50.
				8.8	2.8	31.1	0.0	0.2	0.0	18.8	50.
				11.0	2.8	32.7	0.0	0.1	0.0	42.7	50.

is not a major assumption. Note that we found a b close to, but somewhat lower, than the HERMES value in the E00-108 analysis, and typical parameters of $A = 0.16 \pm 0.04$, and $B = 0.02 \pm 0.02$ to describe the measured ϕ-dependence [3]. As mentioned before, the values of A and B may well not be constants, but rather depend on x, Q^2, z, p_T^2 at lower energies. Our assumption on b, A, and B for have, however, not too large an impact on the count rate estimates.

Lastly, we assumed that the rates for $z > 0.70$ were identical to those at $z = 0.70$, to mimic the fact that the high-z cross sections are underestimated in the E00-108 experiment (see Fig. 3). The coincidence rate estimates, thus calculated, are given in Table VII.

D. Systematic Uncertainties

Since both the SHMS mechanical and optics design, and also the planned SHMS detector package, are essentially a clone of the HMS, we expect to achieve a similar high level of understanding of the SHMS acceptance function and detector properties. Hence, it makes sense to estimate the systematic uncertainties for the proposed measurements based upon the HMS, and/or HMS-SOS performance.

Based upon an impressive database of inclusive (e,e′) Rosenbluth separations spanning the elastic, resonance and deep inelastic scattering regions, we have achieved a typical point-to-point systematic uncertainty of 1.1% for these measurements [18]. For coincidence measurements of the pion form factor with the HMS-SOS combination, we have achieved a point-to-point systematic uncertainty of 1.9% [19]. The latter is mostly due to the relatively poor understood acceptance function of the SOS, with its difficulty to view long, extended targets. Hence, the estimate for the HMS-SHMS combination for 12-GeV pion form factor measurements is 1.6% [20].

In essence, we propose to measure R in deep inelastic (e,e′) measurements with a pion tag here. Compared to inclusive measurements, there will be additional systematics due to the determination of z ($\sim$ the pion momentum) and for corrections in terms of p_T and $cos(\phi)$ dependencies from the measured spectrometer angles. However, the expected dependence is far less than for the more complicated pion form factor measurements. Hence, it stands to reason to expect a systematic uncertainty in the range between 1.1% and 1.6% for these measurements, very comparable to the statistical precision we attempt to achieve.

V. EXPECTED RESULTS AND BEAM TIME REQUEST

We request a total of 40 days of beam time to measure $R = \sigma_L/\sigma_T$ in semi-inclusive deep inelastic scattering as a function of z, Q^2, and p_T^2, covering a region of interest to the general program of SIDIS physics at a 12-GeV JLab. The projected uncertainties for these proposed measurements are given in Fig. 10.

TABLE VII. Proposed Statistics and Required Beam Time for semi-inclusive deep inelastic scattering with π^+ and π^- detection.

x	Q^2 (GeV^2)	z	θ_{pq} (deg)	E (GeV)	I_{beam} (μA)	N^{π^+}	T^{π^+} (hours)	N^{π^-}	T^{π^-} (hours)	R/A
0.20	2.0	0.30	0.	6.6	25	5k	1.3	5k	2.1	∼1/1
				8.8	25	5k	1.0	5k	1.0	∼1/1
				11.0	25	5k	1.0	5k	1.0	∼1/1
0.20	2.0	0.40	0.	6.6	25	5k	1.7	5k	3.3	∼1/1
				8.8	25	5k	1.0	5k	1.0	∼1/1
				11.0	25	5k	1.0	5k	1.0	∼1/1
0.20	2.0	0.50	0.	6.6	25	5k	2.4	5k	5.6	∼1/1
				8.8	25	5k	1.0	5k	1.0	∼1/1
				11.0	25	5k	1.0	5k	1.0	∼1/1
0.20	2.0	0.65	0.	6.6	50	5k	4.2	5k	13.6	∼1/1
				8.8	25	5k	1.0	5k	1.2	∼1/1
				11.0	25	5k	1.0	5k	1.0	∼1.5/1
0.20	2.0	0.85	0.	6.6	50	10k	5.4	10k	19.5	∼1/1
				8.8	50	10k	1.0	10k	1.6	∼1/1
				11.0	50	10k	1.0	10k	1.0	∼1/1
0.40	4.0	0.30	0.	6.6	25	5k	6.2	5k	10.5	∼1/1
				8.8	25	5k	1.0	5k	1.0	∼3/1
				11.0	50	10k	1.0	10k	1.0	∼1/1
0.40	4.0	0.40	0.	6.6	50	5k	9.0	5k	18.7	∼1.5/1
				8.8	25	10k	1.0	10k	1.6	∼1/1
				11.0	50	10k	1.0	10k	1.0	∼1/1
0.40	4.0	0.50	0.	6.6	50	10k	13.4	10k	34.1	∼1/1
				8.8	50	10k	1.2	10k	3.0	∼1/1
				11.0	50	10k	1.0	10k	1.0	∼1/1
0.40	4.0	0.65	0.	6.6	50	5k	13.0	5k	47.5	∼1/1
				8.8	50	10k	2.3	10k	8.4	∼1/1
				11.0	50	10k	1.0	10k	2.3	∼1.5/1
0.40	4.0	0.85	0.	6.6	50	5k	17.3	5k	71.3	∼2/1
				8.8	50	10k	3.0	10k	12.6	∼20/1
				11.0	50	10k	1.0	10k	3.4	∼10/1
0.15	1.5	0.50	0.	6.6	15	3k	1.4	3k	3.2	∼1/1
				8.8	15	3k	1.0	3k	1.0	∼3/1
				11.0	15	3k	1.0	3k	1.0	∼4/1
0.50	5.0	0.50	0.	6.6	50	5k	16.0	5k	42.0	∼1/1
				8.8	50	10k	2.8	10k	7.5	∼1.5/1
				11.0	50	10k	1.0	10k	2.0	∼10/1
0.30	3.0	0.50	-2.	6.6	25	2.5k	3.0	2.5k	7.4	∼1/1
				8.8	25	5k	1.0	5k	1.3	∼1/1
				11.0	50	10k	1.0	10k	1.0	∼3/1
0.30	3.0	0.50	5.	6.6	50	5k	3.6	5k	8.8	∼1/1
				8.8	50	10k	1.0	10k	1.5	∼2/1
				11.0	50	10k	1.0	10k	1.0	∼3/1
0.30	3.0	0.50	10.	6.6	50	5k	6.8	5k	16.7	∼3/1
				8.8	50	10k	1.2	10k	2.9	∼9/1
				11.0	50	10k	1.0	10k	1.0	∼10/1
0.30	3.0	0.50	15.	6.6	50	2.5k	9.5	2.5k	23.7	∼10/1
				8.8	50	10k	3.3	10k	8.2	∼20/1
				11.0	50	10k	1.0	10k	2.2	∼30/1
0.30	3.0	0.50	20.	6.6	50	2.5k	39.7	2.5k	97.7	∼10/1
				8.8	50	5k	6.8	5k	16.9	∼80/1
				11.0	50	10k	3.7	10k	9.1	∼100/1

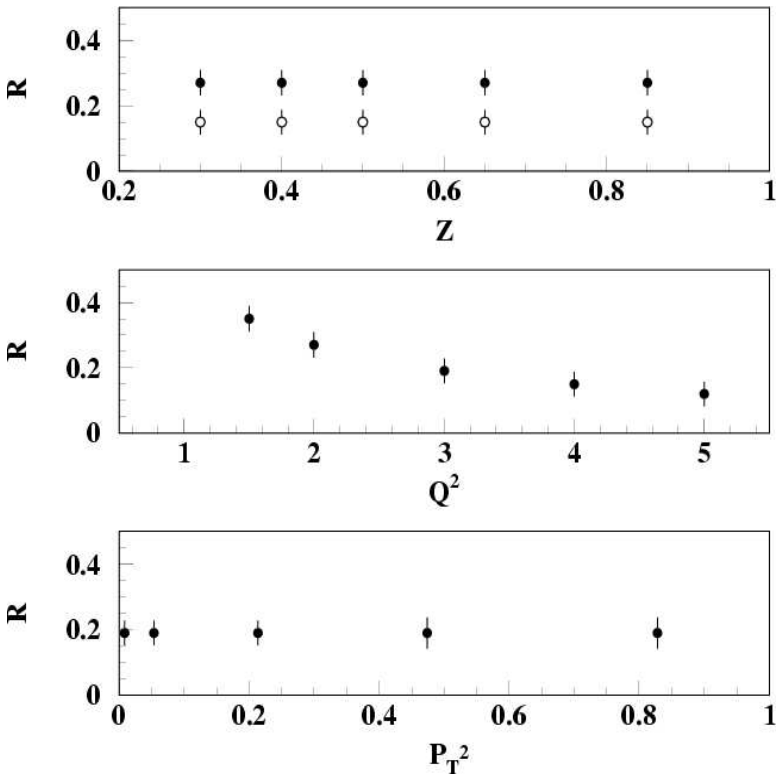

FIG. 10. Projected uncertainties for the proposed measurements. We used R as measured in deep inelastic scattering as ansatz.

TABLE VIII. BEAM TIME REQUEST

E (GeV)	Target	Time (Hours)
6.6	LH2	580
	LD2	59
	Al	58
8.8	LH2	102
	LD2	11
	Al	10
11.0	LH2	51
	LD2	10
	Al	5
	Checkout	24
	Kinematic Changes (50)	25
	Target Changes (67)	12
	Pass Changes (2)	8
	Beam Energy Measurements (3)	6
	Total Request	961

A summary of our beam time request is given in Table VIII, and amounts to 40 days. The beam current for deuterium running will be adjusted such that the singles rates are similar to those for hydrogen. Hence, the produced physics statistics will be almost identical. We assume to run 10% of the time on the Al "dummy" target, for subtraction of end-wall purposes. Time for checkout and configuration changes has been outlined.

A. Contributions to the Base Equipment of Hall C

The Yerevan group (H. Mkrtchyan *et al.*) intends to seek the required calorimeter blocks for the SHMS, refurbish them if needed, and commit to building, checking, installing, and commissioning this calorimeter. In one option, blocks of the existing HERMES calorimeter would be refurbished. In another option, the SHMS calorimeter would be a combination of recycled and new calorimeter blocks. The Yerevan group has already been instrumental in balancing various design options for this calorimeter. The full-time equivalent of the contribution of the Yerevan group is up to 3 FTE's.

The Hampton group (C. Keppel, R. Ent *et al.*) are committed to seek NSF funding, with other local and minority- or undergrad-serving universities, for the main trigger and tracking detectors of the SHMS. In collaboration with William and Mary, Norfolk State, North Carolina A&T, Florida International University and James Madison University, Hampton is preparing a Major Research Instrumentation (MRI) proposal to the National Science Foundation to obtain the necessary funding. Hampton commits, in collaboration with the Norfolk State group, to build the SHMS drift chambers.

REFERENCES

[1] V. Tvaskis *et al.*, to be submitted; E99-118 experiment, spokespersons: A. Bruell, J. Dunne, and C.E. Keppel.

[2] B. Badelek, J. Kwiecinski, and A. Stasto, Z. Phys. **C74**, 297 (1997).

[3] T. Navasardyan *et al.*, to be submitted (also see Appendix); E00-108 experiment, spokespersons: R. Ent, H. Mkrtchyan, and G. Niculescu.

[4] B. Hommez, Ph.D. Dissertation, Gent University (2003), unpublished.

[5] M. Tytgat, Ph.D. Dissertation, Gent University (2001), unpublished.

[6] S.J. Brodsky, L. Frankfurt, J.F. Gunion, A.H. Mueller, and M. Strikman, Phys. Rev. D **50**, 3134 (1994).

[7] J. Collins, L. Frankfurt, and M. Strikman, Phys. Rev. D **56**, 2982 (1997).

[8] L.L. Frankfurt, P.V. Pobylitsa, M.V. Polyakov, and M. Strikman, Phys. Rev. D **60**, 014010 (1999).

[9] M. Diehl, T. Gousset, B. Pire, and O. Teryaev, Phys. Rev. Lett. **81**, 1782 (1998).

[10] X. Ji, Phys. Rev. Lett. **78**, 610 (1997); Phys. Rev. D **55**, 7114 (1997).

[11] A.V. Radyushkin, Phys. Lett. **B380**, 417 (1996); Phys. Rev. D **56**, 5524 (1997).

[12] J.D. Bjorken and J.B. Kogut, Phys. Rev. D **8** (1973) 1341.

[13] R. Asaturyan *et al.*, Nucl. Instr. and Meth. **A548**, 364 (2005).

[14] D.E. Wiser, Ph.D thesis, U. Wisconsin, 1977 (unpublished).

[15] H.L. Lai *et al.*, Eur. Phys. J. **C12** (2000) 375.

[16] J. Binnewies, B. A. Kniehl, and G. Kramer, Phys. Rev. D **52** (1995) 4947.

[17] P. Geiger, Ph.D. Dissertation, Heidelberg University (1998), unpublished.

[18] Y. Liang *et al.*, nuc-ex/0410027; E94-110 experiment, spokesperson: C.E. Keppel.

[19] T. Horn *et al.*, to be submitted; E01-004 experiment, spokespersons: H.P. Blok, G.M. Huber and D. Mack.

[20] *Measurement of the Charged Pion Form Factor to High* Q^2, PAC-30 proposal, spokerspersons: G.M. Huber and D. Gaskell.

The Onset of Quark-Hadron Duality in Pion Electroproduction

T. Navasardyan,[1] G.S. Adams,[2] A. Ahmidouch,[3] T. Angelescu,[4] J. Arrington,[5] R. Asaturyan,[1] O.K. Baker,[6,7] N. Benmouna,[9] C. Bertoncini,[10] H.P. Blok,[11] W.U. Boeglin,[12] P.E. Bosted,[13] H. Breuer,[8] M.E. Christy,[6] S.H. Connell,[14] Y. Cui,[15] M.M. Dalton,[14] S. Danagoulian,[3] D. Day,[16] T. Dodario,[15] J.A. Dunne,[17] D. Dutta,[18] N. El Khayari,[15] R. Ent,[7] H.C. Fenker,[7] V.V. Frolov,[19] L. Gan,[20] D. Gaskell,[7] K. Hafidi,[5] W. Hinton,[6,7] R.J. Holt,[5] T. Horn,[8] G.M. Huber,[21] E. Hungerford,[15] X. Jiang,[22] M. Jones,[7] K. Joo,[23] N. Kalantarians,[14] J.J. Kelly,[8] C.E. Keppel,[6,7] E.R. Kinney,[24] V. Kubarovski,[2] Y. Li,[15] Y. Liang,[25] S. Malace,[4] P. Markowitz,[12] E. McGrath,[26] P. McKee,[16] D.G. Meekins,[7] H. Mkrtchyan,[1] B. Moziak,[2] G. Niculescu,[16] I. Niculescu,[26] A.K. Opper,[25] T. Ostapenko,[27] P. Reimer,[5] J. Reinhold,[12] J. Roche,[7] S.E. Rock,[13] E. Schulte,[5] E. Segbefia,[6] C. Smith,[16] G.R. Smith,[7] P. Stoler,[2] V. Tadevosyan,[1] L. Tang,[6,7] M. Ungaro,[2] A. Uzzle,[6] S. Vidakovic,[21] A. Villano,[2] W.F. Vulcan,[7] M. Wang,[13] G. Warren,[7] F. Wesselmann,[16] B. Wojtsekhowski,[7] S.A. Wood,[7] C. Xu,[21] L. Yuan,[6] X. Zheng,[5] H.Zhu[16]

[1] *Yerevan Physics Institute, Yerevan, Armenia*
[2] *Rensselaer Polytechnic Institute, Troy, New York 12180*
[3] *North Carolina A & T State University, Greensboro, North Carolina 27411*
[4] *Bucharest University, Bucharest, Romania*
[5] *Argonne National Laboratory, Argonne, Illinois 60439*
[6] *Hampton University, Hampton, Virginia 23668*
[7] *Thomas Jefferson National Accelerator Facility, Newport News, Virginia 23606*
[8] *University of Maryland, College Park, Maryland 20742*
[9] *The George Washington University, Washington, D.C. 20052*
[10] *Vassar College, Poughkeepsie, New York 12604*
[11] *Vrije Universiteit, 1081 HV Amsterdam, The Netherlands*
[12] *Florida International University, University Park, Florida 33199*
[13] *University of Massachusetts Amherst, Amherst, Massachusetts 01003*
[14] *University of the Witwatersrand, Johannesburg, South Africa*
[15] *University of Houston, Houston, TX 77204*
[16] *University of Virginia, Charlottesville, Virginia 22901*
[17] *Mississippi State University, Mississippi State, Mississippi 39762*
[18] *Triangle Universities Nuclear Laboratory and Duke University, Durham, North Carolina 27708*
[19] *California Institute of Technology, Pasadena, California 91125*
[20] *University of North Carolina Wilmington, Wilmington, North Carolina 28403*
[21] *University of Regina, Regina, Saskatchewan, Canada, S4S 0A2*
[22] *Rutgers, The State University of New Jersey, Piscataway, New Jersey, 08855*
[23] *University of Connecticut, Storrs, Connecticut 06269*
[24] *University of Colorado at Boulder, Boulder, Colorado 80309*
[25] *Ohio University, Athens, Ohio 45071*
[26] *James Madison University, Harrisonburg, Virginia 22807*
[27] *Gettysburg College, Gettysburg, Pennsylvania 18103*

(July 6, 2006)

The Quark-Hadron Duality phenomenon is well established in both inclusive electron scattering and electron-positron annihilation, and has subsequently been predicted for high-energy hadron electroproduction. A large data set of pion electroproduction from both hydrogen and deuterium targets has been obtained spanning the nucleon resonance region. These data conclusively show the onset of quark-hadron duality, and the relation of this phenomenon to the high-energy factorization ansatz of subsequent electron-quark scattering and quark → pion production mechanisms.

Some three decades after the inception of Quantum Chromodynamics (QCD) as the accepted theory for strong interactions, mysteries remain. At high energies, the property of QCD known as asymptotic freedom allows for an efficient description in terms of quarks and gluons — or partons, weakly interacting at short distances. In contrast, at low energies the effects of confinement impose a more efficient description in terms of collective degrees of freedom, the physical mesons and baryons — or hadrons.

Despite this apparent dichotomy, in nature there exist instances where low-energy hadronic phenomena, averaged over appropriate energy intervals [1], closely resemble those at asymptotically high energies, calculated in terms of quark-gluon degrees of freedom. This is referred to as quark-hadron duality, and reflects the relationship

between the strong and weak interaction limits of QCD — confinement and asymptotic freedom.

The observation of this phenomenon in fact preceded QCD by a decade or so, with the profound discovery of the remarkable relationship between the low-energy cross sections and high-energy behavior in hadronic reactions, with the former on average appearing to mimic features of the latter. At that time, this was explained with the development of Finite Energy Sum Rules, relating dispersion integrals over resonance amplitudes at low energies to Regge parameters describing the high-energy scattering [2]. The equivalence, on average, of hadron production in electron-positron annihilation and the underlying quark-antiquark production mechanism was later similarly understood [3]. Due to confinement, of course, quarks and antiquarks must end up as hadrons.

It was natural, therefore, that the early observation of quark-hadron duality between resonance production and the high-energy continuum in inclusive electron-nucleon scattering was also interpreted within this framework. Bloom & Gilman found that by averaging the proton F_2 structure function data over an appropriate energy range the resulting structure function in the resonance region closely resembled the scaling function which described the high-energy scattering of electrons from point-like partons [4]. Recently, the phenomenon has been revisited with unprecedented precision, with striking results: Quark-hadron duality occurs at much lower values of momentum transfer squared, Q^2, and in far less limited regions of energy than could have been expected [5].

Although postulated to be a general property of QCD, the dynamical origin of quark-hadron duality remains poorly understood. It should manifest itself in a wide variety of processes and observables. In this Letter, we generalize the duality concept to the unexplored region of ("semi-inclusive") pion electroproduction [6,7], $eN \rightarrow e\pi^{\pm}X$, in which a charged pion is detected in coincidence with a scattered electron. The missing mass of the residual system X squared, M_x^2, will be in the nucleon resonance region for the remainder of this Letter, and we will show the dual behavior of this region with a high-energy parton description.

At high energies, one expects from perturbative QCD that there will be factorization between the virtual photon–quark interaction and the subsequent quark hadronization,

$$\frac{\frac{d\sigma}{d\Omega_e dE_e dz dp_T^2 d\phi}}{\frac{d\sigma}{d\Omega_e dE_e}} = \frac{dN}{dz} b e^{-bp_T^2} \frac{1 + A\cos(\phi) + B\cos(2\phi)}{2\pi}, \quad (1)$$

$$\frac{dN}{dz} \sim \sum_q e_q^2 \; q(x, Q^2) \; D_{q\rightarrow\pi}(z, Q^2), \quad (2)$$

where the fragmentation function $D_{q\rightarrow\pi}(z, Q^2)$ gives the probability for a quark to evolve into a pion π detected with a fraction z of the quark (or virtual photon) energy, $z = E_\pi/\nu$. The transverse momentum p_T, z and the angle ϕ reflect the extra kinematical degree of freedom associated with the pion momentum, with b the average transverse momentum of the struck quark. At very high energies, the factors A and B become zero. The parton distribution functions $q(x, Q^2)$ are the usual functions depending on the Bjorken variable x and the four-momentum transfer squared Q^2. A consequence of this factorization is that the fragmentation function is independent of x, and the parton distribution function is independent of z. Both the parton distribution functions and the fragmentation functions, however, depend on Q^2 through logarithmic Q^2 evolution.

At lower energies, it is not obvious that the pion electroproduction process factorizes in the same manner as in Eq. (2). At energies where hadronic phenomena dominate, the pion electroproduction process may rather be described through the excitation of nucleon resonances, N^*, and their subsequent decays into mesons and lower lying resonances, N'^* [17]. For the quark-hadron duality phenomenon to occur, non-trivial cancellations of the angular distributions from various decay channels [18,19] are required to produce the fast-forward moving pion of the high-energy limit.

The experiment (E00-108) ran in the summer of 2003 in Hall C at Jefferson Lab. An electron beam with a current varying between 20 and 60 μA was provided by the CEBAF accelerator with a beam energy of 5.5 GeV. Incident electrons were scattered from a 4-cm-long liquid hydrogen or deuterium target and detected in the Short Orbit Spectrometer (SOS). The SOS central momentum remained constant throughout the experiment, with a value of 1.7 GeV. The electroproduced mesons (predominantly pions) were detected in the High Momentum Spectrometer (HMS), with momenta ranging from 1.3 to 4.1 GeV/c. The experiment consisted of two parts: i) at a fixed electron kinematics of $(x, Q^2) = (0.32, 2.30\ \mathrm{GeV}^2)$ the central HMS momentum was varied to cover a range of $0.3 < z < 1.0$; and ii) similarly, at $z = 0.55$, the electron scattering angle was varied, at constant momentum transfer angle, to span a range in x from 0.22 to 0.58. Note that this corresponds to an increase in Q^2, from 1.5 to 4.2 GeV^2. All measurements were performed for both positively-charged π^+ and negatively-charged π^-.

Events from the aluminum walls of the cryogenic target cell were subtracted by performing substitute empty target runs. Scattered electrons were selected by the use of both a gas Cherenkov counter and an electromagnetic calorimeter. Pions were selected using the coincidence time difference between scattered electrons and secondary hadrons. In addition, an Aerogel detector was used for pion identification [20]. For kinematics with pion momenta above 2.4 GeV a correction was made to remove kaons from the pion sample, 10% in the worst case (at $z \sim 1$), as determined from the electron-hadron coincidence time. From a measurement detecting positrons

in SOS in coincidence with pions in HMS, we found the background originating from π^0 production and its subsequent decay into two photons and then electron-positron pairs, negligible.

We have added the possibility of semi-inclusive pion electroproduction to the general Hall C Monte Carlo package SIMC [21], following the high-energy expectation of Eq. (2). We used the CTEQ5 next-to-leading-order (NLO) parton distribution functions to parameterize $q(x,Q^2)$ [22], and the fragmentation function parameterization for $D^+_{q\rightarrow\pi}(z,Q^2)+D^-_{q\rightarrow\pi}(z,Q^2)$, with D^+ (D^-) the favored (unfavored) fragmentation function, from Binnewies *et al.* [23]. The remaining unknowns are the ratio of D^-/D^+, the slope b of the p_T dependence, and the parameters A and B describing the ϕ dependence. Both the D^-/D^+ ratio [24] and the b-value [25] are taken from HERMES analyses.

We can not constrain b well within our own data set due to the limited (p_T,ϕ) acceptance of a magnetic spectrometer setup. Our best estimate is $b = 4.0 \pm 0.4$, with no noticable differences between b-values extracted from the p_T-dependence of either π^+ and π^- data, or ^{1}H and ^{2}H data. This is somewhat lower than the slope b of the p_T dependence reported by the HERMES collaboration ($b \approx 4.66$) [25]. We do find a ϕ dependence in our data, with typical parameters of $A = 0.16 \pm 0.04$, and $B = 0.02 \pm 0.02$. These ϕ-dependences become smaller to negligible in the ratios of cross sections shown later. Similarly, we find a Q^2-dependence in our data that differs from the factorized high-energy expectation, but again this will not affect the results shown below. Of course, these findings do cast doubt on the strict applicability of the high-energy approximation for our experiment.

Within our Monte Carlo package, we estimated two non-trivial corrections to the data. Radiative corrections were applied in two steps. We directly estimated the radiation tails within our semi-inclusive pion electroproduction data using the Monte Carlo. In addition, we explicitly subtracted radiation events coming from the exclusive reactions $e+p \rightarrow e'+\pi^+ +n$ and $e+n \rightarrow e'+\pi^- +p$. For these processes, we interpolated between the low-W^2, low-Q^2 predictions using the MAID model [26] and the higher-W^2 data of Brauel *et al.* and Bebek *et al.* [27,28]. We subtracted events from diffractive ρ production, using PYTHIA [29] to estimate the p(e,e$'\rho^\circ$)p cross section with similar modifications as implemented by the HERMES collaboration [25,30]. Note that we also made a small 2% correction to the deuterium data to account for a small Final-State Interaction effect of the pions traversing the deuterium nucleus [31].

The ^{1,2}H(e,e$'\pi^\pm$)X cross sections as measured at $x = 0.32$ are compared with the results of the simulation in Fig. 1, as a function of z. The general agreement between data and Monte Carlo is excellent for $z < 0.65$. Within our kinematics ($p_T \sim 0$), M_x^2 is almost directly related to z, as $M_x^2 = M_p^2 + Q^2(1/x-1)(1-z)$. Hence, the large "rise" in the data with respect to the simulation at $z > 0.8$ mainly reflects the $N-\Delta(1232)$ region. Indeed, if one considers a ^{1}H(e,e$'\pi^-$)X spectrum as function of missing mass of the residual system X, one sees only one prominent resonance region, the $N-\Delta$ region. Apparently, above $M_x^2 = 2.5$ GeV^2 or so, there are already sufficient resonances to render a spectrum mimicking the smooth z-dependence as expected from the Monte Carlo simulation following the factorization ansatz of Eq. (2).

To quantify the surprising resemblance of semi-inclusive pion electroproduction data in the nucleon resonance region with the high energy prediction of Eq. (2), we formed simple ratios of the measured cross sections, insensitive to the fragmentation process (assuming charge symmetry) at leading order (LO) in α_s. If one neglects strange quarks and any p_T-dependence to the parton distribution functions, these ratios can be expressed in terms of u and d parton distributions, as follows

$$\frac{\sigma_p(\pi^+)+\sigma_p(\pi^-)}{\sigma_d(\pi^+)+\sigma_d(\pi^-)} = \frac{4u(x)+4\bar{u}(x)+d(x)+\bar{d}(x)}{5(u(x)+d(x)+\bar{u}(x)+\bar{d}(x))}, \quad (3)$$

$$\frac{\sigma_p(\pi^+)-\sigma_p(\pi^-)}{\sigma_d(\pi^+)-\sigma_d(\pi^-)} = \frac{4u_v(x)-d_v(x)}{3(u_v(x)+d_v(x))}, \quad (4)$$

with the notation $\sigma_p(\pi^+)$ refering to the π^+ pion electroproduction cross section off the proton, $u = u_v + \bar{u}$, $d = d_v + \bar{d}$, and the Q^2-dependence left out of these formulas for convenience. These ratios allow us to study the factorization ansatz in more detail, with both ratios rendering results independent of z (and p_T).

We show our results for these ratios in Fig. 2, with the solid (open) symbols reflecting the data after (before) subtraction of the diffractive ρ contributions. The shaded area reflects the expectation under the assumptions described above (LO, no strange quark effects, charge symmetry for the fragmentation functions). We included in these shaded areas a variety of calculations, using both LO and NLO ($M\bar{S}$ and valence) parton distribution functions from the GRV collaboration, and NLO calculations from the CTEQ collaboration [16,22].

Our data are remarkably close to the near-independence of z as expected in the high-energy limit, with the clearest deviations in the region of $z > 0.7$, approaching on the $N-\Delta$ resonance region. Within 10% we find perfect agreement beyond this region, although our excellent statistics allows to also see clear deviations within this limit. *E.g.*, our data seem non-statistically distributed around the high-energy expectation for the first ratio, outside our systematic uncertainties (indicated with the crossed areas).

Using the deuterium data only, the ratio of unfavored to favored fragmentation functions D^-/D^+ can be extracted. This ratio is, to a good approximation, at LO simply given by

$$D^-/D^+ = \left(4 - \frac{\sigma_d(\pi^+)}{\sigma_d(\pi^-)}\right) / \left(4\,\frac{\sigma_d(\pi^+)}{\sigma_d(\pi^-)} - 1\right). \quad (5)$$

In the high-energy limit, this ratio should solely depend on z (and Q^2), but not on x. The results are shown in Fig. 3, with the closed (open) symbols reflecting the data after (before) subtraction of the diffractive ρ contributions. The solid curves are a fit to the HERMES data for the same ratio [24]. The dashed curve is the expectation $(1-z)/(1+z)$ according to Field and Feynman for independent fragmentation [32]. The crossed areas indicate the systematic uncertainties, dominated by uncertainties due to the two non-trivial corrections discussed above.

We observe that the extracted values for D^-/D^+ closely resemble those of the HERMES experiment [24]. The data show a near-independence as a function of x, as expected from Eq. (2), and a smooth slope as a function of z, reflecting a fit to the higher-energy HERMES data, all at $M_x^2 > 4$ GeV^2. This is quite remarkable given that our data cover the full resonance region, $M_p^2 < M_x^2 < 4.2$ GeV^2. Apparently, there is a mechanism at work that removes the resonance excitations in the π^+/π^- ratio, and hence the D^-/D^+ ratio. This mechanism can be simply understood in the SU(6) symmetric quark model. We note that both our data and the fit to the higher-energy HERMES data far exceed the Feynman and Field expectations for large z.

Close & Isgur [19] applied the SU(6) symmetric quark model to calculate production rates in various channels in semi-inclusive pion photoproduction, $\gamma N \to \pi X$. The pattern of constructive and destructive interference, which was a crucial feature of the appearance of duality in inclusive structure functions, is in this model also repeated in the semi-inclusive case. The results suggest an explanation for the smooth behavior of $D^-/D^+ \equiv D_d^{\pi^+}/D_u^{\pi^+}$ for a deuterium target in Fig. 3. The relative weights of the photoproduction matrix elements, summed over p and n, is for π^+ production always 4 times larger than for π^- production. In the SU(6) limit, therefore, the resonance contributions to the ratio of Eq. (5) cancel exactly, leaving behind only the smooth background, as would be expected at high energies. This may account for the glaring lack of resonance structure in the resonance region fragmentation functions in Fig. 3.

In summary, we have measured charged-pion ($\pi^\pm$) electroproduction cross sections in the resonance region for both hydrogen and deuterium targets. We observe, for the first time, the quark-hadron duality phenomenon in such reactions. Several ratios constructed from these data exhibit, at low energies, the features of factorization in a sequential electron-quark scattering and a quark-pion fragmentation process. The ratio of favored to unfavored fragmentation functions closely resembles that of high energy reactions, even though our data are solely in the nucleon resonance region. This observation can be explained in the $SU(6)$ symmetric quark model. Quark-hadron duality appears the underlying cause of the smooth transition "on average" from hadrons to quarks witnessed in nature, allowing simple quark-gluon descriptions of observables down to relatively low-energy scales.

The authors wish to thank A Bruell, C.E. Carlson and W. Melnitchouk for helpful discussions. This work is supported in part by research grants from the U.S. Department of Energy and the U.S. National Science Foundation. The Southeastern Universities Research Association operates the Thomas Jefferson National Accelerator Facility under the U.S. Department of Energy contract DEAC05-84ER40150.

[1] E.C. Poggio, H.R. Quinn and S. Weinberg, Phys. Rev. D **13** (1976) 1958.
[2] M Fukugita and K Igi, Physics Reports **31** (1977) 237.
[3] I.I.Y. Bigi and N. Uraltsev, Int. J. Mod. Phys. **A 16** (2001) 5201.
[4] E.D. Bloom and F.J. Gilman, Phys. Rev. D **4** (1971) 2901; E.D. Bloom and F.J. Gilman, Phys. Rev. Lett. **25** (1970) 1140.
[5] I. Niculescu *et al.*, Phys. Rev. Lett. **85** (2000) 1186; Phys. Rev. Lett. **85** (2000) 1182.
[6] C.K. Chen, SLAC-PUB-1469, Aug. 1974 (unpublished).
[7] A. Afanasev, C.E. Carlson and C. Wahlquist, Phys. Rev. D **62** (2000) 074011.
[8] E. L. Berger, Nucl. Phys. **B85** (1975) 61.
[9] E. L. Berger, Proc. of the Workshop on Electronuclear Physics with Internal Targets, Stanford, California, January 5-8, 1987.
[10] P. J. Mulders, hep-ph/0010199 (2000).
[11] C. J. Bebek *et al.*, Phys. Rev. Lett. **34** (1975) 759; Phys. Rev. Lett. **37** (1976) 1525; Phys. Rev. D **15** (1977) 3085.
[12] C. J. Bebek *et al.*, Nucl. Phys. **B75** (1974) 20.
[13] J.M. Scarr *et al.*, Nucl. Phys. **B135** (1978) 224.
[14] A. Calogeracos, N. Dombey, and G. B. West, Phys. Rev. D **51** (1995) 6075.
[15] P. Eden, P. Hoyer and A. Khodjamirian, JHEP 0110 (2001) 040; P. Hoyer, hep-ph/0208190.
[16] M. Glück, E. Reya, and A. Vogt, Eur. Phys. J. **C5** (1998) 461.
[17] W. Melnitchouk, AIP Conf. Proc. **588** (2001) 267.
[18] N. Isgur, S. Jeschonnek, W. Melnitchouk and J.W. Van Orden, Phys. Rev. D **64** (2001) 054005.
[19] F.E. Close and N. Isgur, Phys. Lett. **B 509** (2001) 81.
[20] R. Asaturyan *et al.*, Nucl. Instrum. Meth. **A548** (2005) 364.
[21] D. Gaskell, private communications. See also http://www.jlab.org/Hall-C/.
[22] H.L. Lai *et al.*, Eur. Phys. J. **C12** (2000) 375.
[23] J. Binnewies, B. A. Kniehl, and G. Kramer, Phys. Rev. D **52** (1995) 4947.
[24] P. Geiger, Ph.D. Dissertation, Heidelberg University (1998), unpublished.
[25] B. Hommez, Ph.D. Dissertation, Gent University (2003),

unpublished.
[26] D. Drechsel, S.S. Kamalov, and L. Tiator Nucl. Phys. **A645** (1999) 145.
[27] P. Brauel *et al.*, Z. Physik C **3** (1979) 101.
[28] C.J. Bebek *et al.*, Phys. Rev. D **17** (1978) 1693.
[29] T. Sjostrand, L. Lonnblad, S. Mrenna, and P. Skands, hep-ph/0308153 (2003).
[30] M. Tytgat, Ph.D. Dissertation, Gent University (2001), unpublished.
[31] M.M. Sargsyan, private communications (2005).
[32] R.D. Field and R.P. Feynman, Nucl. Phys. **B136** (1978) 1.
[33] M. Arneodo *et al.*, Nucl. Phys. **B321** (1989) 541.

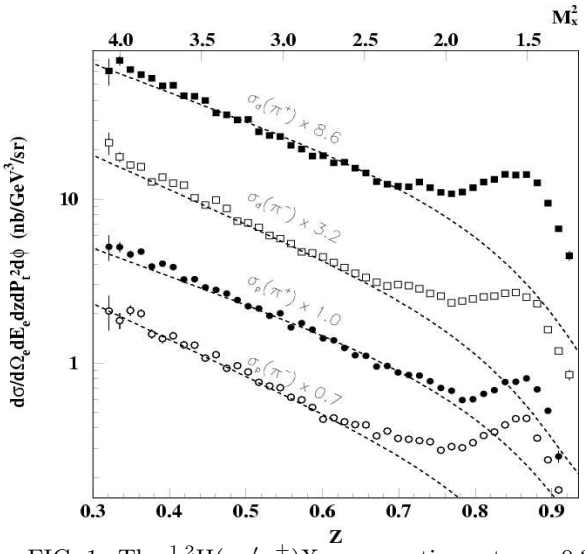

FIG. 1. The ^{1,2}H(e,e′$\pi^{\pm}$)X cross sections at $x = 0.32$ as a function of z in comparison with Monte Carlo simulations (dashed curves) starting from a fragmentation ansatz (see text). The various cross sections have been multiplied as indicated for the purpose of plotting.

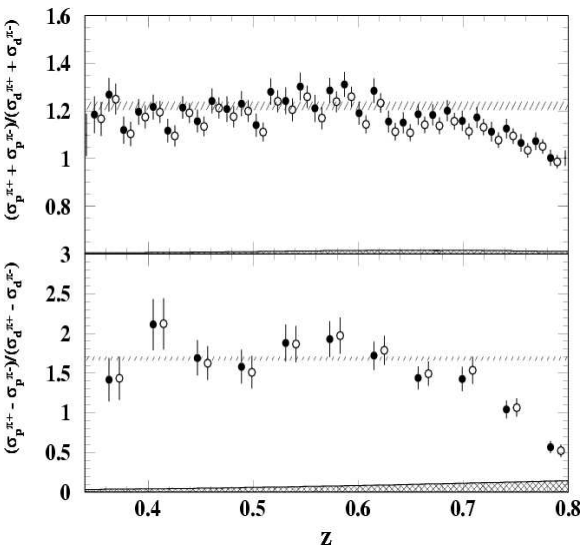

FIG. 2. The ratio of proton to deuterium results of the sum (top) and difference (bottom) of π^+ and π^- cross sections as a function of z, at $x = 0.32$. Closed (open) symbols reflect data after (before) events from coherent ρ production are subtracted (see text). The symbols have been sightly offset in z for clarity. The shaded area represents a variety of calculations, at both leading order and next-to-leading-order of α_s, of the shown ratio, neglecting strange quarks, and assuming charge symmetry for the fragmentation functions and parton distributions [16,22].

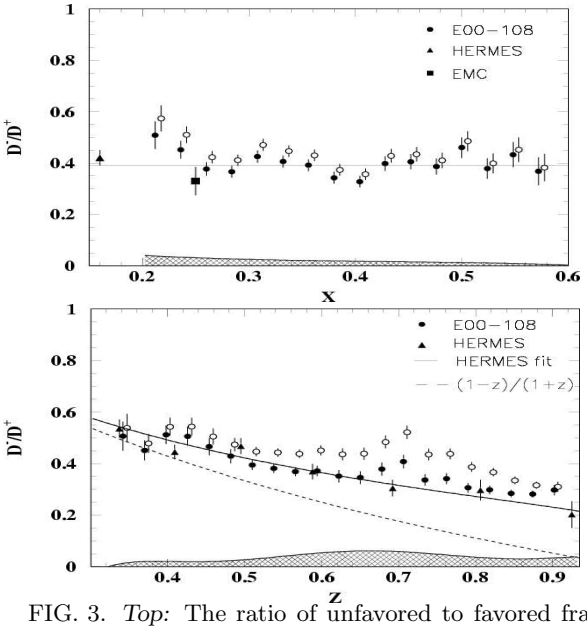

FIG. 3. *Top:* The ratio of unfavored to favored fragmentation function D^-/D^+ as a function of x at $z = 0.55$, evaluated at Leading Order from the deuterium data. Closed (open) symbols reflect data after (before) events from coherent ρ production are subtracted (see text). The symbols have been slightly offset in x for clarity. The solid curve represents the value from the HERMES fit [25]. Further, the ratio is shown as determined by EMC (square) [33]. *Bottom:* Same as *top*, but now as a function of z for $x = 0.32$. The dashed curve represents an early expectation [32] under the independent fragmentation hypothesis.